Polymer Testing 117 (2023) 107859

Contents lists available at ScienceDirect

Polymer Testing

journal homepage: www.elsevier.com/locate/polytest

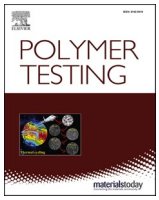

Open challenges in tensile testing of additively manufactured polymers: A literature survey and a case study in fused filament fabrication

Antonella Sola [a,*], Wei Juene Chong [a,b], Dejana Pejak Simunec [a], Yuncang Li [b], Adrian Trinchi [a], Ilias (Louis) Kyratzis [a], Cuie Wen [b,**]

[a] CSIRO Manufacturing Business Unit, Clayton, Victoria, 3169, Australia
[b] School of Engineering, RMIT University, Melbourne, Victoria, 3001, Australia

ARTICLE INFO

Keywords:
Tensile properties
International standard
Size effect
Additive manufacturing
Fused filament fabrication
Fused deposition modeling

ABSTRACT

Additive manufacturing (AM, also commonly termed 3D printing) is progressing from being a rapid prototyping tool to serving as pillar of the Industry 4.0 revolution. Thanks to their low density and ease of printing, polymers are receiving increasing interest for the fabrication of structural and lightweight parts. Nonetheless, the lack of appropriate standards, specifically conceived to consistently verify the tensile properties of polymer parts and benchmark them against conventional products, is a major obstacle to the wider uptake of polymer AM in industry. After reviewing the standardisation needs in AM with a focus on mechanical testing, the paper closely examines the hurdles that are encountered when existing standards are applied to measure the tensile properties of polymer parts fabricated by fused filament fabrication (FFF, aka fused deposition modeling, FDM), which is presently the most popular material extrusion AM technique. Existing standards are unable to account for the numerous printing parameters that govern the mechanical response of FFF parts. Moreover, the literature suggests that the raster- and layer-induced anisotropic behaviour and the complicated interplay between structural features at different length scales (micro/meso/macro-structure) undermine pre-existing concepts regarding the specimen geometry and classical theories regarding the size effect, and ultimately jeopardise the transferability of conventional tensile test standards to FFF parts. Finally, the statistical analysis of the tensile properties of poly (lactic acid) (PLA) FFF specimens printed according to different standards (ASTM D638 type I and ASTM D3039) and in different sizes provides experimental evidence to confirm the literature-based argumentation. Ultimately, the literature survey, supported by the experimental results, demonstrates that, until dedicated standards become available, existing standards for tensile testing should be applied to FFF with prudence. Whilst not specified in conventional standards, set-up and printing parameters should be fully reported to ensure the repeatability of the results, rectangular geometries should be preferred to dumbbell-like ones in order to avoid premature failure at the fillets, and the size of the specimens should not be changed arbitrarily.

1. Introduction

Additive manufacturing (AM) is gradually subverting the paradigms of fabrication, especially in industrial sectors, such as aerospace and medicine, that require a high level of customisation and extreme geometric complexity. In contrast to subtractive processes that remove material from a larger original bulk, AM technologies gradually build up three-dimensional (3D) objects through the selective addition of material, mainly in a layer-wise manner. This enables the tool-less production of intricate patterns and bespoke designs. Oftentimes, as stated in ISO/ASTM 52900 [1] (note: for brevity, hereafter full bibliographic information of standards will only be referenced at their first occurrence), the fabrication of parts through the deposition of a material using a print head, nozzle or another printer technology is also termed “3D printing”. Especially in non-technical contexts, the two terms are used as synonyms. The name 3D printing is also increasingly common in the scientific literature, in parallel with the emerging field of 4D printing, which is the additive manufacture of 3D components and devices whose shape or function change over time (which is therefore the 4th dimension) in response to an external stimulus [2].

* Corresponding author. CSIRO Manufacturing BU, Private Bag 10, Clayton South, VIC, 3169 Australia.
** Corresponding author. School of Engineering, RMIT University, GPO Box 2476, Melbourne VIC, 3001, Australia.
E-mail addresses: antonella.sola@csiro.au (A. Sola), cuie.wen@rmit.edu.au (C. Wen).

https://doi.org/10.1016/j.polymertesting.2022.107859
Received 4 September 2022; Received in revised form 13 October 2022; Accepted 3 November 2022
Available online 4 November 2022

As recently summarised by Kabir et al. [3], AM is still in its infancy, with the first patent for a commercial 3D printer (a stereolithography apparatus, SLA, belonging to the vat photopolymerisation family, "VPP", as per ISO/ASTM 52900) being issued in 1986. For this reason, there has been limited progress so far in the standardisation and metrology in AM [4,5]. To date, much attention has been dedicated to the advancement of standards and testing protocols for metal-based AM parts. Owing to their mechanical properties, metals are often preferred to polymers and ceramics in load-bearing applications. The development of standards and specifications for metal-based AM components has thus been perceived as a priority in order to enable their safe usage for structural purposes [6–17]. However, AM is a fast-growing field of research, and the need for established guidelines to measure the mechanical and functional properties of AM parts produced with new materials and processes poses substantial challenges beyond the qualification and certification of metal-based systems [5,18,19]. For example, Hollister et al. [20] provided a detailed analysis of the regulatory issues that developers may experience when translating 3D printed polymer scaffolds from academic research to clinical practice and identified the lack of qualification and certification standards as a major reason for potential delays in achieving the final approval from the regulator (in this case, the Food and Drug Administration, FDA). On the other hand, it has been demonstrated that fibre-reinforced polymer parts produced by fused filament fabrication (FFF, aka fused deposition modeling, FDM, which is nowadays the most popular material extrusion AM technique, “MEX” as per ISO/ASTM 52900) can exceed the specific strength of aluminium 6061–0, which means that emerging polymer-based systems are ideal candidates for replacing metals in load-bearing lightweight structures [21].

One of the main gaps in existing standards regards the determination of the tensile properties of AM parts. Tensile tests are by far the most commonly applied mechanical tests in the literature, and they are also very popular in industrial practice. Although this is untold, tensile tests are often seen as “the” mechanical tests, tout court. Various factors contribute to the wide acceptance of tensile tests. The procedure is relatively easy and short. In terms of conventional fabrication methods, tensile samples do not need a substantial amount of material, and international standards also account for “small samples”. The required equipment is relatively affordable and small, which means that it does not require major facilities, and many research and development (R&D) labs in industry and academia can perform their tensile tests internally. On the other hand, if properly conducted and interpreted, tensile tests carry rich information regarding the mechanical properties of a material, including its brittle or ductile behaviour, “stiffness” (Young’s modulus), yield strength (if any), maximum and ultimate tensile strength, and elongation at break [10,22]. Although several exceptions exist (for example, fibres and composites may prematurely fail under compression due to buckling and production-related defects [23,24]), most materials exhibit a higher strength under compressive stress than under tensile stress [25], and therefore the tensile strength can be often assumed as a lower bound for the compressive strength. For example, Ahn et al. [26] characterised the mechanical behaviour of acrylonitrile-butadiene-styrene (ABS) parts and reached the conclusion that the maximum compression strength of FFF specimens is approximately two times as much as the tensile strength.

Not surprisingly, as reported by Monzón et al. [27], the first attempt to develop a specific standard in the field of AM was focused on tensile testing for “rapid prototyped” specimens. However, the work on this standard, originally conducted by the E28.16 Rapid Prototyping Subcommittee of the American Society for Testing and Materials (ASTM International, abbreviated hereafter as ASTM) E28 Mechanical Testing Committee, was interrupted in 2009, when it was decided to start a new ASTM committee specifically dedicated to AM, and the draft was never finalised [27].Whereas several papers in the literature summarise the progress in standardisation for AM, the main goal of the present review is to draw attention to tensile testing, which appears to be a major need on account of the huge popularity of this characterisation method. FFF is considered here as a paradigm in order to outline the difficulties that may emerge in tensile testing of AM parts. FFF deserves particular consideration because there is a remarkable disparity between the limited information available in the literature regarding the reliable characterisation of FFF parts, and the extraordinary success of this technique in industry, in academia, and even in home settings, to the point that, according to recent statistics [28], FFF is ranked the most widespread AM method worldwide. The increasing awareness that reliable characterisation methods are needed to enable the safe adoption of FFF parts and grab a deeper understanding of their behaviour is demonstrated by the emerging body of literature dedicated to this subject. Besides the overwhelming number of research articles investigating the relationship between printing parameters and tensile response, more and more papers are critically discussing the appropriateness of existing standards and suggesting avenues to overcoming their limitations. In 2015, Forster [29] published an accurate analysis of the existing standards for measuring the mechanical properties and failure of polymers and polymer-matrix composites and, for each of them, assessed the applicability to AM testing. Basically, out of 44 standards, only 27 were classified as “applicable with guidance”, meaning that their applicability could be limited and needing additional considerations. None of the standards reviewed by Forster was endorsed as immediately applicable, and the remaining 17 were assessed as non-applicable at all. Very recently, Phillips et al. [30] critically reviewed the current methods followed for preparing tensile test specimens and proposed guidelines for implementing them in a new standard. The review published by Phillips et al. [30] highlights the role of the printing parameters and especially the slicing procedure, with the final recommendation that a new dedicated standard for tensile testing should account for all these variables. However, there is still a lack of understanding about the reasons why existing standards fail to reliably capture the tensile response of FFF parts. The main goal of the present review is to bridge this gap and elucidate the consequences of the raster-based deposition of material on the elusive tensile behaviour of FFF parts. Owing to the raster-based deposition of material that is the basis of FFF, printed parts exhibit a hierarchical architecture that makes the processing-structure-properties-performance (PSPP) relationships difficult to control, negates the suitability of classical testing geometries and undermines the validity of conventional scaling theories. The role of the specimen size is thoroughly examined, and further investigated experimentally. Size-related effects in FFF have not been systematically reviewed so far, and yet they are worthy of great attention. As demonstrated in this research, even relatively small changes in size, such that tensile test specimens still comply with the reference standard, are sufficient to make a statistically relevant difference to the measured tensile properties.

Ultimately, it is envisaged that gaining a deeper understanding of the deficiencies of current standards will contribute to the development of future dedicated standards that more effectively measure the tensile behaviour of FFF parts. Until then, as thoroughly examined in this research, it is critical to identify why current standards are unsuitable to test FFF parts and, wherever possible, formulate appropriate mitigation strategies.

2. Outline

As highlighted in this review, the absence of specific standards for testing the tensile properties of FFF parts is a serious gap needing urgent attention. However, this is part of a bigger problem, since the need for standardisation negatively impacts all areas of AM. Accordingly, this review opens up with an introductory section regarding the “Standardisation of testing protocols in AM” (Section 3), which contextualises the tensile testing issues in the bigger picture of the AM standardisation issues. Next, the paper concentrates on FFF. In Section 4, after describing the build-up mechanisms that underpin the structure of FFF parts, the

paper clearly identifies the main reasons for the inadequacy of existing standards to determine the tensile properties in FFF. Firstly, conventional standards are unable to account for the numerous variables (printer type and set-up, processing parameters, environmental conditions, etc.) that affect the mechanical behaviour of FFF parts. Secondly, although the dumbbell-like geometry described in ASTM D638 and ISO 527–2 is prevailing in the literature, premature failure is likely to occur at the filleta, and this calls into question the suitability of conventional testing geometries (section 5). Lastly, the hierarchical structure of FFF parts undermines the validity of classical scaling theories. For the sake of completeness, non-standardised testing procedures are also presented, as they provide additional insight into tensile testing issues. Additional testing parameters, such as the strain rate, are taken into consideration, as they can affect the obtained experimental results. In order to support the major findings reached through the literature survey, the paper proceeds with a case study related to the evaluation of the tensile properties of poly(lactic acid) (PLA) parts printed by FFF (Section 5). The accurate statistical analysis demonstrates that the measured tensile properties change with the specimen size and geometry, even if all samples conform with existing standards, namely ASTM D638 type I and ASTM D3039. As pointed out in the discussion (section 6), the unsuitability of existing standards originates from the multi-scale inner architecture of FFF constructs. At present, the non-transferability of current standards to FFF constructs ultimately leads to the paradoxical conclusion that the properties of FFF parts tested "according to the standard" can hardly be compared, verified, or benchmarked against archival data, even if very common materials are in use like PLA. In conclusion (section 7), until dedicated standards become available, existing standards for tensile testing should be applied to FFF with cautiousness. Printer set-up and printing conditions should be fully reported alongside the testing parameters to ensure the repeatability of the results. Rectangular specimens should be preferred to curvilinear ones with varying cross section in ordet to meet the failure acceptance criteria, and a standard size should be adopted. If, for any reason, this is unpractical, detailed information regarding the specimen size should also be provided.

3. Standardisation of testing protocols in AM

3.1. The need for standardisation

Generally speaking, standardisation is required to enable the reliable flow of goods and services between buyer and seller through the adoption of a common terminology ("language") and of established rules and protocols. For international standards, the goods and services exchange should ideally stretch across different countries. The timely formulation of dedicated standards is particularly important for emerging technologies like AM, as standards can provide clarity, benchmark new products and systems against pre-existing ones, and facilitate their acceptance in the marketplace [31].

Adopting consistent testing protocols is necessary to compare the properties of parts produced with different feedstock materials or under different printing conditions. Thanks to a sound and meaningful comparison, materials engineers and developers can assess the printability of new materials, industrial stakeholders can confidently choose among different feedstocks for balancing costs and performance, and final users can verify the quality of their printed parts against the properties declared in technical data sheets [10,31,32].

Though not strictly pertaining to mechanical characterisation, standardised geometrical artifacts are needed to reliably compare the "performance" of different AM systems, or to monitor the consistency of the "performance" of the same AM system over time, where "performance" refers here to the printing accuracy in linear and circular geometries, to the resolution in printing ribs, pins, holes and slots, and to the surface texture and roughness [11,33]. This need has been met by ISO/ASTM 52902 [34] that presents 8 different artifact geometries (including linear and circular shapes for "accuracy"; pins, holes, ribs and slots for "resolution"; "Surface texture"; volumetric X and Y letters for "labelling") that can be variously combined in order to evaluate the capability of AM systems and to calibrate them, as recently reviewed by de Pastre et al. [35].

Testing goods and services according to established protocols is also key in product qualification and certification. Although standards are adopted on a voluntary basis, using them to formally demonstrate that a product has successfully been tested for performance and quality assurance proves that the product meets the criteria outlined in regulations, specifications, or contracts, in addition to satisfying the expectations of both the manufacturer and the end user [36]. Product qualification and certification are particularly demanding in those fields where a component's failure may have catastrophic consequences and even pose human lives at risk, such as in aerospace, aviation, automotive, and biomedical industries [32]. For example, according to the policy of the federal aviation administration (FAA), a product for commercial aviation must undergo three consecutive certifications before being approved as compliant with regulations, namely: the "Type Certificate", which confirms the design adequateness; the "Production Certificate", which demonstrates the establishment of a reliable quality control system to repeat the Type Certificate specifications; and ultimately the "Airworthiness Certificate", which grants the component for operation [37]. Although the requirements are different according to the level of criticality of the part (details have been reviewed by Seifi et al. [15]), the whole certification process is extremely laborious and the estimated time to completion may be as long as 10–15 years, even in case conventional materials and processes are in use [14,32]. In order to facilitate the completion of the "Type Certificate" step, archival data for approved reference materials can be applied instead of real experimental values. However, if new materials or new processes are introduced, reference data does not exist, and experimental testing is thus required. Acquiring enough information for the statistical validation of mechanical properties for structural components may need up to 10,000 test samples [37]. A crucial point in this regard is that dedicated standards, specifically formulated for AM parts, are still missing and therefore it may be very challenging to demonstrate that the claimed performance has been achieved and can be consistently reproduced.

Some companies have established internal proprietary processes for qualification and quality control, including testing protocols. However, due to intellectual property hurdles, details are rarely disclosed. Moreover, in the community there may be a lack of consensus towards protocols that are company- and application-specific [13]. The advancement of standardisation is thus set to be an enabling factor for fostering the wider adoption of AM in industry, especially in safety critical fields [32].

3.2. Applicability of existing standards to AM

It is generally accepted that existing standards and procedures for testing conventional materials and processes cannot be automatically translated to AM [32]. As critically discussed by Monzón et al. [27], the adoption of standards originally conceived for conventional materials and processes is subject to two basic conditions being met: "Are the existing standards suitable for AM?" and "Do these existing standards respond to AM's specific characteristics?". Quite often, the response is negative [27]. As a result, most existing standards cannot be applied to AM. Sometimes, existing standards can be extended to AM, but guidance is needed to account for some potential hurdles, such as the unsuitability of the prescribed specimen size, geometry, or accuracy [8,16,29]. Since existing standards have been conceived for testing conventional materials and processes, they may prescribe specimen specifications that are unpractical for AM [15]. Moreover, since AM is a very dynamic field of research, different technologies may have different technology readiness levels (RTLs). It has been argued that dumbbell-like samples complying with existing standards for tensile testing, and even prismatic

coupons matching strict tolerances, may be too difficult to be printed with experimental technologies that may initially come with software and hardware limitations [38]. On the other hand, many commercial printers are built as "black boxes", where the hardware and software cannot be modified, and the operator is not allowed to change the printing parameters freely [39]. This means that there might be technical limitations to the feasibility of prescribed specimens, especially if fine tuning of the printing conditions and hardware is required.

In terms of mechanical properties, several factors contribute to the unsuitability of existing standards for testing AM parts. As stated by Roach and Gardner [12], an essential feature of AM is that material and part are created simultaneously. This brings into question the real significance of testing the mechanical properties of a 3D printed object, as the obtained experimental values reflect the performance of the part, rather than the property of the material. In other terms, a shift in mentality is needed, as the effect of material and architecture cannot be separated in AM [12]. According to the definition applied by Meza and Greer [40], AM test specimens can thus be regarded as "architectured materials". Following sections of this paper scrutinise this concept taking FFF as representative example.

As already discussed by Monzón [27] and reinstated by Bae et al. [32], another major obstacle to the simple adoption of existing standards comes from the extreme variability encountered in AM parts. For example, with regard to polymer-based AM, many parameters are involved in the printing process, and they can all affect the mechanical properties of the printed parts [41]. The properties of plastic-based parts can be substantially different according to the 3D printing technology in use (for instance, thermoplastic parts can be manufactured by FFF and by selective laser sintering (SLS, belonging to the powder bed fusion, "PBF", family according to ISO/ASTM 52900) with sensibly different results in terms of microstructure and related properties [42]), the feedstock material (for example, filaments for FFF coming from different manufacturers may have experienced different thermal histories, which leads to filaments having different properties in spite of the nominal composition being the same [43]), the specific processing parameters (for example, the layer thickness is generally reported to affect the ultimate tensile strength of FFF parts, but the induced change can be either positive or negative depending on the part orientation on the base platform [44]), and the possible need for post-processing (for example, parts produced by FFF may be used as printed, but they may also receive post-printing treatments such as heating, chemical finishing, or machining [45,46]).

In particular, testing methods formulated for conventional materials are often unable to account for the anisotropy of AM parts that originates from the layer-wise build-up mechanisms [4,27,47]. A possible way around this consists in repeating the test on samples built under different orientations. In principle, this would allow the anisotropic response of AM parts to be fully identified [15]. However, printing tensile specimens parallel to the growth direction can be difficult due to the limited capability of most 3D printers [48]. Moreover, multiplying the number of tests unavoidably increases the material consumption, which may be critical with experimental feedstocks (generally produced in small volume batches) or other costly materials. The necessity of repeating the test along different directions would also increase the time for testing and, ultimately, slow down the qualification process, which may be a substantial hindrance for those industries, like aerospace, that are turning to AM in the hope for shorter design, development, and lead times with respect to conventional manufacturing [13]. On the other hand, the lengthiness of conventional avenues of testing has already been identified as a major hurdle that clashes with the vision of AM as a fast fabrication pathway [8,49]. Another difficulty coming from the multi-directional testing strategy is the complexity of the obtained data, as it is still unclear how the direction-dependent values should be captured for design purposes [15,50]. Seifi et al. [15] argued that the simplest approach would be to describe the material as being isotropic and responding as observed along the weakest direction. However, this approach may be even too conservative in some circumstances [15]. As discussed in the following sections, anisotropy-related issues are emphasised in some techniques like FFF, where anisotropy may be induced by several mechanisms, and not just by the layer-by-layer deposition of material.

Another major hurdle to the adoption of existing standards comes from the microstructural randomness of AM parts. It is well known that AM components are affected by erratic defects and microstructural features that cannot be identically reproduced from part to part even if the feedstock material, the processing parameters, and the environmental conditions are the same [51]. In this regard, a workshop jointly organized by ASTM and the National Institute of Standards and Technology (NIST, U.S. Department of Commerce) in 2016 identified statistical variation as one of the most important factors hindering the determination of sound and reproducible PSPP relationships (illustrated in Fig. 1) in metal-based AM [8].

Since microstructural defects are randomly generated in AM parts, mechanical properties are likely to experience sensible and unpredictable fluctuations. As compared to conventional materials and processes, a statistical approach to defining "average" properties in AM may thus need a much larger batch of samples to be tested [15]. Moreover, these microstructural defects may undermine the fatigue resistance and durability of AM components. For this reason, as described by Seifi et al. [15], the FAA (in addition to conventional fatigue tests and fracture analysis) has outlined a statistical approach based on the frequency of occurrence and the size distribution of material anomalies. This information is then elaborated to define an "exceedance curve" of material anomalies and ultimately fed into a probabilistic model of fracture mechanics. The random appearance of defects in AM basically undermines the validity of conventional standardised destructive test methods that are often based on the assumption of material homogeneity [15].

Another point to consider is that the requirements for qualification and certification, and hence the tests to be conducted, may be different for different applications, for example in automotive, spacecraft, and biomedical devices [8,15,18]. This means that, whilst some standards and specifications may still address AM as whole (for example, standards describing AM classification and terminology, such as ISO/ASTM 52900 that defines "Additive manufacturing — General principles — Fundamentals and vocabulary"), quite often specific rules and guidelines should be issued to assist in different businesses [15,18]. As such, new standards in AM are now simultaneously required in multiple industries [15].

Discussion is still open regarding the usefulness of printing coupons and witness samples for testing purposes [7,15,52,53]. As reviewed by Crocker [7], ASTM F2971 [54] includes general directions for 3D printing witness specimens for tensile testing. Witness samples should be machined from bulk-deposition near-net-shape components and built in four orientations (X, Y, XY, and Z) in accordance with ISO/ASTM 52921 [55]. Their location within the build volume should also be reported. However, Ferrell et al. [18] argued that ASTM F2971 is rarely applied in the literature, especially with regard to FFF. According to Ferrell et al. [18], the vague reporting requirements for the specimen fabrication and the inability to account for all possible orientations and printing configurations achievable through FFF are the main reasons for the limited adoption of this standard. In a broader perspective, beyond the specificities of FFF, the microstructure and hence the properties of a printed part are strongly dependent on local building conditions, and especially on the thermal history, that are influenced by the part geometry and size, and not just by its orientation and location on the base platform [7,8,15,53,56]. Since the local printing environment can be sensibly different from part to part, it is questionable that the properties, as measured on coupons or on witness samples, might be truly representative of the behaviour of more complicated (or just diverse) structures [7,8,15,53]. Likewise, the distribution of thermal stresses after printing is closely related to the part shape, dimensions, and orientation [57,58].

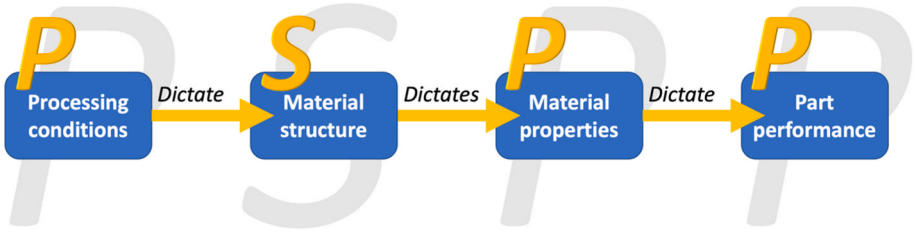

Fig. 1. Relationships between processing conditions (P), material structure (S), material properties (P) and part performance (P), PSPP, according to the definition given by Hrabe et al. [8].

On the other hand, testing each individual part is unfeasible, destructive tests cannot be applied to one-of-a-kind parts, and even non-destructive evaluation (for example, by X-ray computed tomography) to verify structural integrity may be not applicable to special parts, for example because they may too big or too thick [13].

These difficulties represent substantial barriers that hinder the adoption of existing standards in AM and suggest that a new regulatory framework is needed.

3.3. Development of new standards for AM: A work in progress

3.3.1. Main bodies contributing to the standardisation of materials and processing in AM

As recently reviewed by Udroiu et al. [33], there are currently three main organisations working worldwide on the standardisation of materials and processing in AM (aka Standards Developing Organisations, SDOs), namely the International Organization for Standardization (ISO), with technical committee ISO/TC 261 (active since 2011), the ASTM, with group ASTM F42 (since 2009), and the European Committee for Standardization (CEN), with technical committee CEN/TC 438 (since 2015).

Officially started in 2018, the ASTM International Additive Manufacturing Center of Excellence (AM CoE) is a collaborative partnership among ASTM and representatives from government, academia, and industry. The main goal of AM CoE is to conduct strategic research and development (R&D) to promote the advancement of standards across all aspects of AM and thus to promote the adoption of AM in all industries (further details can be found in the contribution by Gumpinger et al. [31]). Whilst AM CoE is currently running several projects covering all fields of standardisation in AM, it is worth noting that Project 1805: Polymer AM test specimen design (having the National Institute of Aviation Research (NIAR) as Responsible Partner) is specifically focused on mechanical testing issues observed in polymer AM [59].

In the United States, other federal agencies have been involved in the standardisation of AM, including the National Science Foundation (NSF), the Office of Naval Research (ONR), and the NIST [9]. NIST-led workshops have enabled the development of "Measurement Science Roadmaps" that explore the existing challenges in science and metrology of both metal- and polymer-based AM ("Measurement science roadmap for metal-based additive manufacturing" [60] and "Measurement science roadmap for polymer-based additive manufacturing" [61]). The importance and the practicality of these roadmaps are widely recognised in the literature (as summarised, for example, by Bae et al. [32] and by Chua et al. [39]), on account of the extensive participation in these activities from industry, academia, and government.

Following to a technical meeting in October 2015, America Makes and the American National Standards Institute (ANSI) started the Additive Manufacturing Standardization Collaborative (AMSC), also supported by federal agencies including NIST, NASA, FAA and the Department of Defence. Although the AMSC is not called to issue new standards, its role is to coordinate the regulatory efforts in the United States as clarified through the AMSC standardisation roadmap published in 2018 [62].

3.3.2. ISO and ASTM standards

Back in 2011, ISO and ASTM International signed the Partner Standards Development Organization (PSDO) cooperative agreement, whose main goal was to coordinate the efforts between ASTM Committee F42 on Additive Manufacturing Technologies and ISO Technical Committee 261 on Additive Manufacturing [63]. In 2016, under the PSDO umbrella the two organisations jointly approved the Additive Manufacturing Standards Development Structure, which is an international framework helping experts and standardisation bodies interact globally. As stated in the official announcement from ISO [64], it is envisaged that this joint plan will set the foundation for internationally accepted standardisation in AM, through the identification and the prioritisation of existing gaps, and through the coordination of available resources to avoid overlaps, duplications and potential incongruences between standards targeting similar topics [65]. Meanwhile, already existing standards and protocols are assessed for commonalities and, wherever possible, merged into more coherent guidelines. The main goal of standards harmonisation is thus to simplify and clarify existing information, in order to reduce the complexity and cost of part qualification and certification in AM [32].

Following to the Vienna agreement with ISO/TC 261, CEN Technical committee TC438 also publishes the ISO (and ISO/ASTM) standards as EN ISO (EN ISO/ASTM) standards in order to promote the consistent adoption of international standards in European countries (further detail regarding the structure of working groups targeting the standardisation of AM across ISO, ASTM and CEN has been recently published by Martínez-García et al. [36]).

In the framework of the PSDO agreement, new standards are issued according to a three-level hierarchical structure (as reported by Naden [64]) comprising of (i) General AM standards, (ii) Category AM standards, and (iii) Specialised AM standards. It is intuitive that the philosophy underpinning this classification system is the "specificity" of standards, meaning that general AM standards apply to all AM materials and processes (for example, the definition of AM terminology); category AM standards are more specific, and regulate materials and processes within specific categories (for example, polymer filaments); lastly, specialised AM standards focus on particular materials and processes (for example, ABS filaments) [36].

As of September 2022, 6 standards are listed for ASTM Subcommittee F42.01 on Test Methods, i.e. ISO/ASTM 52921, ASTM F2971, ISO/ASTM52902, ASTM ISO/ASTM 52907 [66], ASTM F3571 [67], and ASTM F3122 [68]. ISO/ASTM 52921 and ASTM F2971 are general AM standards. While ISO/ASTM 52921 describes the standard terminology for coordinate systems and test methodologies, ASTM F2971 provides standard guidelines for reporting data for AM test specimens. According to Bae et al. [32], ASTM F2971 can be regarded as the first step towards the establishment of materials databases and repositories to collect valid data in standardised format. It has been often claimed that a database gathering information about material properties, process parameters and defects, would bring to light the PSPP relationships in AM, enable the straightforward comparison of different feedstocks, and facilitate the adoption of existing AM materials on new machines [8,32,39].

As previously mentioned, ISO/ASTM52902 provides guidance regarding test artifacts for the assessment of the geometric capability of AM systems.

ASTM ISO/ASTM 52907, ASTM F3571, and ASTM F3122 are category AM standards applying to metals. In particular, ASTM ISO/ASTM 52907 covers the experimental methods to characterise metallic powders, whilst ASTM F3571 details how to characterise the shape of metal powders using automated static or dynamic image analysis by optical photography. Interestingly, ASTM F3122 should serve as a guide to existing standards (or their variations) that may be applicable to determine the mechanical properties of metal parts produced by AM. As noted by Bae et al. [32], this standard acknowledges that the results of mechanical tests conducted on AM parts according to existing protocols may be affected by numerous variables, including feedstock material, material anisotropy, method of material preparation, part's porosity, method of specimen preparation, testing environment, specimen alignment and clamping, testing speed, and testing temperature.

Some additional standards by ISO/TC 261 Technical Committee address the characterisation of AM parts. For example, ISO 27547–1 [69] describes the preparation of test specimens of thermoplastic materials using "mouldless technologies", with a focus on laser sintering, while the very recent ISO/ASTM TR 52906 [70] has been issued to serve as a best practice for the identification and intentional seeding of flaws for non-destructive testing of metal parts. ISO 17296–3 [71], which belongs to the ISO 17296 series providing general principles in AM, includes tensile tests among the test methods relevant for the mechanical characterisation of AM parts. However, ISO 17296–3 just redirects to existing standards as the consultation documents for specimen geometry and test procedures.

Presently, none of the existing international standards specifically describes how to conduct tensile tests on AM parts. In the following sections, FFF will serve as an example of the challenges currently encountered in tensile testing while a dedicated standard is still missing.

4. Challenges in tensile testing of FFF parts: literature findings

The complexity of the mechanical behaviour of FFF parts and, hence, the inadequacy of conventional standards to reliably measure their tensile properties originate from the build-up mechanisms, whereby FFF parts are the result of the progressive addition and consolidation of individual layers along the growth direction, and of individual rasters of material within each layer. As discussed in the following paragraphs, this poses three substantial challenges that undermine the validity of conventional standards for tensile testing. Firstly, existing standards are unable to capture the PSPP relationships in FFF, and to account for the numerous variables in play. Secondly, the raster-based deposition of material does not lend itself to the obtainment of curved geometries with varying cross-sectional area as observed in widespread dumbbell-like tensile specimens. Thirdly, since the raster diameter cannot be miniaturised freely, technical constraints negate the validity of conventional scaling laws. Out-of-standard approaches that target the behaviour of individual rasters or individual layers have also been suggested for estimating the tensile properties of FFF parts. However, as shown below, they still suffer substantial limitations, especially in terms of repeatability. Finally, it should be mentioned that other tensile testing parameters specified in existing standards, such as the strain rate, may be not readily transferable to FFF and may thus need attention from the regulator.

4.1. Build-up mechanisms in FFF

FFF, like all AM techniques, is the combination of digital manufacturing and physical manufacturing. Before printing, the object's geometry must be modelled through computer-aided design (CAD) software or acquired from an existing prototype through computed tomography or other 3D scanning tools (reverse engineering). Next, the design must be converted into a "standard tessellation language" (.stl) file [72]. Over the years, several file formats have been developed for 3D printing, including the "additive manufacturing format" (AFM) jointly managed by ISO/TC 261 and ASTM F42 committees under the ISO/-ASTM 52915 standard [73]. Nonetheless, the .stl format is still prevailing in industry. Then, the.stl file is sliced to 2D sections corresponding to the layers in the physical object. The 2D slices, in their turn, are translated to the G-code that controls the printhead motion and the printing conditions, such as temperature and speed [72].

Typical feedstock materials for FFF are thermoplastics or thermoplastic-matrix composites in the form of filaments having a tightly controlled diameter of 1.75 or 2.85 mm, depending on the printing hardware [74]. As illustrated in Fig. 2, the filament is fed into the printhead by the action of two counter-rotating gears. The core of the printhead is the liquefier, where the feedstock material is heated and melted. The filament at the liquefier's entrance works like a piston and pushes the melt out of the print nozzle. While the extrudate is being deposited on the base platform, the printhead moves on a X–Y gantry following a computer-controlled toolpath defined by the G-code, so that the extrudate draws the cross section of the part. When the first layer is completed, the base platform moves downward along the Z (growth) direction (or, vice versa, the printhead moves upward), and a second layer is added on top of the previous one. The process is then repeated layer by layer until completion of the desired 3D geometry [75].

As commonly observed in most AM technologies, the layer-wise build-up mechanisms and the consequent stratification of layer-layer interfaces induce a strong anisotropy in the growth direction [76–78]. Anisotropic effects in the growth directions may also be worsened by thermal residual stresses, especially for semi-crystalline polymers that experience a substantial shrinkage upon cooling [79]. According to the terminology introduced in Fig. 3, the behaviour of FFF parts is therefore different if they are printed "upright" as opposed to "flat" or "on-edge".

Since the surface of FFF builds is typically rough, post-processing may be needed to improve the surface finish. This may also contribute to mitigating the marks caused by the breakaway of (non-washable) supports required for printing overhanging structures [22], and ultimately influence the mechanical properties of FFF by smoothing off potential crack initiation points [43].

Some equipment configurations may have different mechanisms to produce the relative movement between the printhead and the base platform (for example, in Delta printers the printhead is hinged to three or more arms that slide along vertical rails [80]). However, the basic principle remains the same, with the filament being melted and

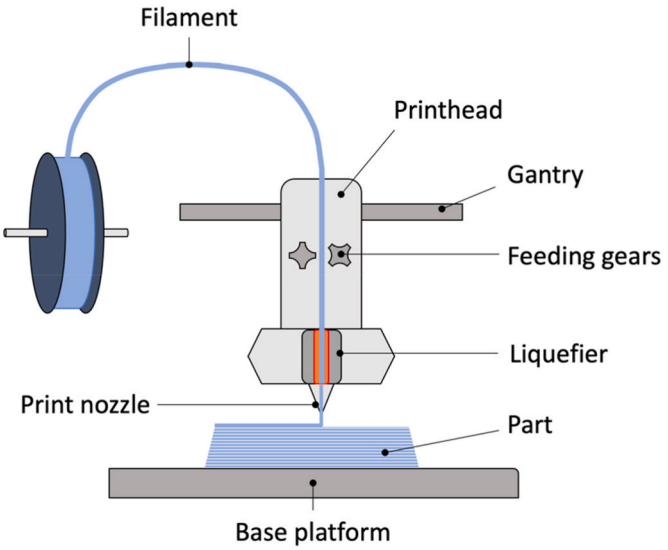

Fig. 2. Schematic representation of an FFF printer.

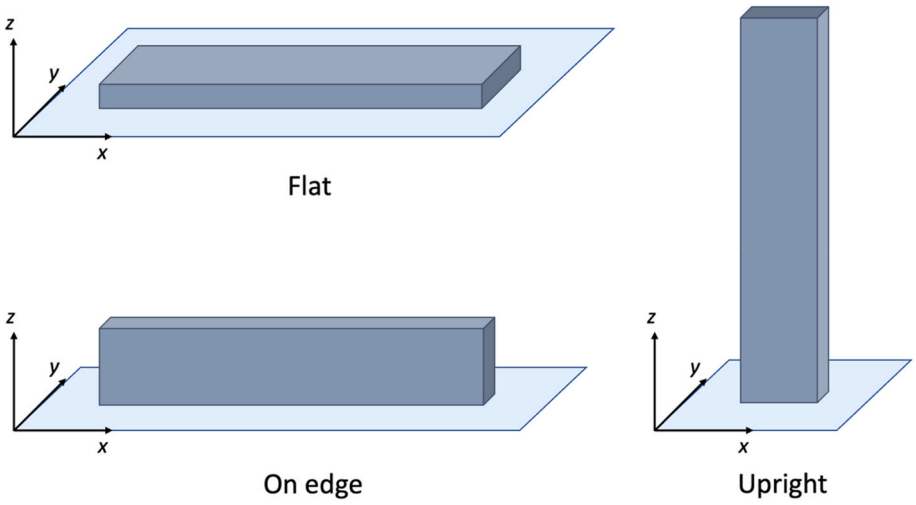

Fig. 3. Same part printed under different orientations as "flat", "on edge" and "upright" on the base platform.

selectively deposited to fabricate the part. Whilst the object as a whole is built up in a layer-by-layer fashion, each layer, in its turn, is actually the result of the progressive addition and welding of multiple string-like beads of material, often called "rasters" or "roads" [75], being extruded next to each other.

The obtainment of a solid part in FFF largely depends on the establishment of structural bonds between neighbouring rasters of material within each layer, as well as on the establishment of structural bonds between subsequent layers [81]. The consolidation mechanisms occurring in FFF are extremely complicated and the discussion in this regard is still open in the literature [75]. Basically, adjacent rasters are joined together through polymer sintering, and then the raster-raster interface is healed through molecular reptation and re-entanglement [82–86]. As schematically presented in Fig. 4, the new raster of material is still in the molten state when it touches the previous one. An equilibrium temperature is reached at the raster-raster interface, and the local increase in temperature activates the motion of the polymer chains also in the previous raster. This triggers the inter-diffusion of polymer molecules across the interface, which is responsible for welding the adjacent rasters. However, it has been estimated that, under normal printing conditions, the interface temperature drops down to below the glass transition temperature in less than 2 s [87], and this prematurely arrests the inter-raster fusion before completion [83,84]. Whereas for amorphous thermoplastics the glass transition temperature is considered the limiting temperature for molecular inter-diffusion to occur, the chain mobility of semi-crystalline thermoplastics is already hindered at the crystallisation temperature, since increasing portions of the polymer macromolecules become pinned in the growing crystalline areas. In principle, it is generally recognised that the presence of well-ordered crystalline regions provides semi-crystalline thermoplastics with superior stiffness, strength, and wear resistance with respect to amorphous polymers [88]. However, in FFF parts this crystallisation-induced strengthening effect can be outbalanced by the weaker bonding at the raster interface [89].

4.2. PSPP relationships in FFF

The raster-based build-up brings about three important consequences on the PSPP relationships in FFF parts.

Firstly, because of the precocious interruption of the interface healing process, the raster-raster interface is typically weaker than the solid material. This largely justifies the in-plane anisotropy observed in FFF parts printed with a linear infill pattern and the key role played by the raster angle in controlling the mechanical properties [90]. The anisotropic effects extend beyond the mechanical behaviour and affect all functional properties, including thermal and electrical conductivity [91,92], that may be sensibly different along different directions.

If the part geometry is elongated, as it happens with tensile testing coupons, and all rasters within each layer are parallel, the "raster angle" defines the direction of the rasters with respect to the main axis of the part, which ultimately coincides with the loading direction in tensile specimens [93]. Fig. 5 illustrates the concept of raster angle for a

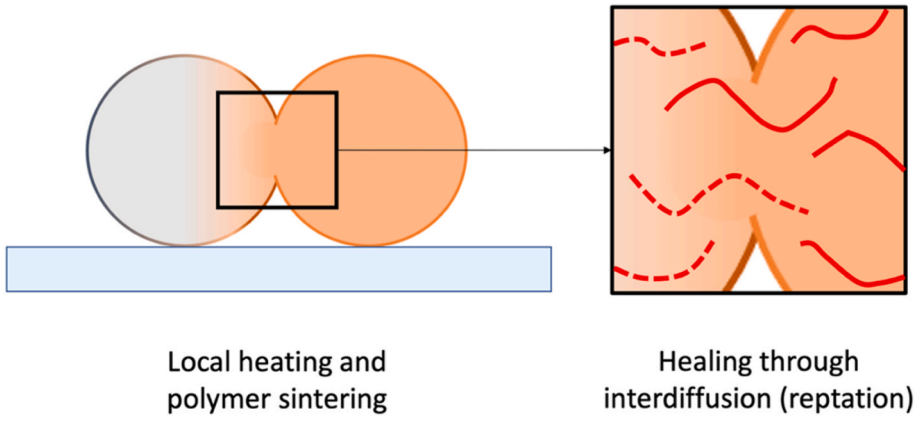

Fig. 4. Consolidation in FFF occurring through local re-heating, polymer sintering and interface healing (polymer chain reptation). The rasters are ideally represented as having round cross section.

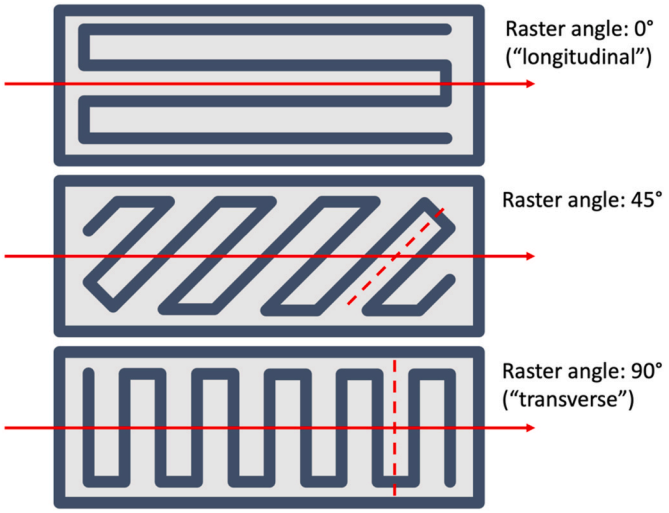

Fig. 5. Same part printed under different raster angles.

relatively simple rectangular geometry. Typically, owing to the structural weakness of inter-raster interfaces, the mechanical (tensile and flexural) strength in the "longitudinal" direction is higher than the "transverse" one.

In fact, in tensile samples printed under a 0° raster angle, the load is applied parallel to the rasters and hence the rasters themselves bear the tensile stresses. However, when the raster angle departs from 0°, an increasing fraction of the applied load is transferred to the raster-raster interfaces, which are structurally weaker, and this reduces the tensile strength of the part. Intuitively, tensile samples printed under a 90° raster angle are subject to the worst conditions, as the tensile stresses act normal to the raster-raster interfaces [90]. To some extent, the raster-based structure of individual layers in FFF parts may be remindful of continuous fibre-reinforced composites, whose mechanical properties are similarly dependant on the relative orientation between the fibres and the loading direction. This analogy between individual layers and orthotropic laminae has inspired several approaches to describing the mechanical behaviour of FFF parts according to the classical laminate theory (CLT) originally formulated for continuous fibre-reinforced laminates [19,94–98]. An interesting outcome of these models is that the anisotropic behaviour can be mitigated at the part level by the design of a balanced stacking sequence, for example by symmetrically alternating +45° and −45° raster angles [94]. However, one of the main limitations of the CLT-based approach is its inability to account for complicated infill patterns, whereby individual layers are not made of linear rasters [50].

Secondly, the tensile behaviour of FFF parts is strongly influenced by the likely presence of voids between adjacent rasters. A very important parameter in this regard is the infill degree that, for a simple infill pattern comprising parallel rasters as shown in Fig. 6, is related to the width of the rasters and to the distance between them. If the infill degree is less than 100%, and hence the relative distance exceeds the raster width, an air gap survives between neighbouring rasters. Taking into account the ability of FFF to print according to a multitude of different infill patterns (not only rectilinear, but also triangular, honeycomb, Hilbert curve, just to name a few [50,99–101]), the concept of infill degree can be generalised as the volume fraction of the part that is actually filled by printing material [102]. It is generally stated that adopting an infill degree lower than 100% reduces the tensile strength [99,103–105]. However, reducing the infill degree does offer some advantages, such as reducing the print time, the part's weight, and the consumption of rare or costly feedstock materials (including experimental ones) [103]. Moreover, parts with a lower infill degree may achieve a higher elongation at break under tensile loading [102],

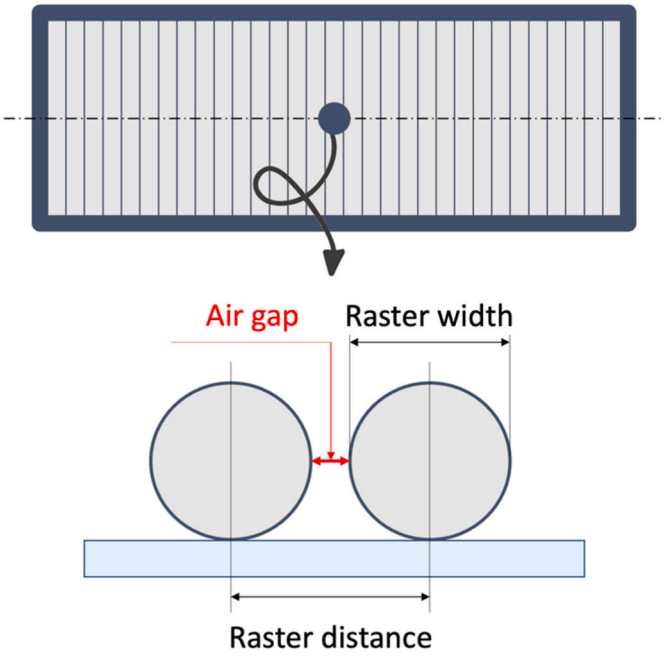

Fig. 6. If the relative distance exceeds the raster width, an air gap remains between neighbouring rasters, thus resulting in an infill degree lower than 100%. The rasters are ideally represented as having round cross section.

because the reduced number of joining nodes leads to a lower defect density [106]. Lightweight structure effects have also been reported in the literature, such that the tensile strength [107–109] and the apparent Young's modulus [106] do not depend linearly on the infill degree. Similar results have also been observed in bending tests, as the flexural strength of the samples printed, for example, with 60% infill degree is higher than 60% of the flexural strength of the same samples printed with 100% infill degree [110].

Even if the infill degree is set to 100%, FFF parts often present large voids at the rasters' junctions due to partial welding. As it leaves the nozzle (which is routinely round, even though other geometries, such as square nozzles, have also been described in the literature for research purposes [111,112]), the strand of material has a circular cross section. However, the extrudate slightly flattens when it touches the base platform or the previous layer, due to the combined action of the force of gravity and the pressure applied by the nozzle [113–115]. Once the printing speed and feeding rates have been fixed, the degree of flattening depends on the ratio between the nozzle diameter (that corresponds to the nominal diameter of the extrudate) and the layer thickness [115]. The layer thickness is routinely fixed to a value lower than ¾ (0.75) of the nozzle diameter (recommended value: ½ (0.5) of the nozzle diameter) [116]. According to Coogan and Kazmer [117], working with a smaller layer thickness increases the exit pressure. As a results, the new layer is effectively pushed into intimate contact with the previous one. However, as discussed by Tao et al. [90], thin layers experience a high cooling rate, which rapidly hinders the polymer chain mobility and impairs the inter-raster bonding. Since decreasing the layer thickness increases both the exit pressure and the number of layers and hence the number of joints, the effect of the layer thickness will ultimately depend on the relative strength of the joints and the feedstock material. If the bond strength is comparable to the material itself, the tensile strength is expected to increase with thinner layers; conversely, if the joints are weaker than the material, the tensile strength is expected to decrease with thinner layers [118]. The degree of flattening is also affected by the molten viscosity and by the molten surface tension of the feedstock material, which in turn depend on the intrinsic properties of the material in use and on the processing temperatures, including the printing

temperature and the temperature of the base platform (in case this is heated) [84,119]. The interplay between the infill degree, the degree of flattening, and the advancement of polymer sintering and healing governs the formation of these inter-raster voids [90]. As shown in Fig. 7, in parts printed under a simple linear infill pattern these voids often resemble long channels running parallel to the deposition direction, with a rhombic or triangular cross section according to the stacking sequence of the layers (aligned vs skewed). The presence of these inter-raster void channels accounts for the common observation that the tensile strength of FFF parts printed under a 0° raster angle is still lower than that of injection moulded counterparts, in spite of the applied load being carried axially by the rasters [81]. In fact, in FFF parts the real load-bearing cross sectional area is lower than the nominal one due to the inter-raster voids. However, this weaking effect in FFF parts may be partly compensated for by the preferential orientation of the polymer chains (and elongated fillers, if present [120]) along the deposition direction [26,44,83,121].

Lastly, it should be mentioned that the inter-raster consolidation mechanisms are influenced by all thermal variables, including thermal history and thermal environment. The local thermal history of a raster is dictated by the printing path, which, in its turn, is controlled through the G-code. As a general rule, if the previous raster is still relatively hot when the new raster touches it, there is more time for polymer healing to progress. On average, the time elapsed between the deposition of subsequent layers is longer than that between neighbouring rasters, which means that the consolidation phenomena along the growth direction are particularly disadvantaged [18]. This is why, as recently pointed out by Gao et al. [81], FFF parts suffer the largest anisotropy in the growth direction among all AM constructs. Besides the thermal history, it is generally recognised that also the "printing environment" temperatures, namely the temperature of the base platform, if heated, and the temperature of the print chamber envelop, if any, play an important role in promoting consolidation [122,123]. Although less obvious, it has been suggested that working under controlled atmosphere may also be beneficial, since printing under low vacuum may reduce the residual porosity [124,125], while the exclusion of oxygen may avoid the degradative effect of polymer oxidation [126]. Taking into account the hygroscopic behaviour of most thermoplastic materials and composites for FFF [127], pre-drying is often necessary and the level of humidity in the atmosphere should also be closely controlled [22,103,106,128–136].

A summary of the parameters affecting the tensile properties of FFF parts is provided in Fig. 8. A detailed analysis of the relationship existing between hardware, printing parameters, and environmental conditions on the one hand, and tensile properties of FFF parts on the other hand, is beyond the scope of the present contribution (and the interested reader can already find numerous reviews and research articles that extensively discuss this topic, for instance in Refs. [18,26,44,50,52,106,137–152]). Nonetheless, the role of these numerous variables should be emphasised in this context in order to demonstrate that standardised testing procedures should account for the specific parameters and conditions that are applied when building the tensile specimens. Unlike conventional manufacturing processes, when it comes to FFF (and, in broader terms, to AM) the same part, if printed with different printing parameters or with a different printer or under different ambient conditions, may show different tensile properties, even if the feedstock filament is the same [18,153]. This also leads to the conclusion that, if FFF parts are tested according to existing standards, the printer in use, the environmental conditions, and the specific printing parameters chosen to print the parts should be declared, otherwise the mere indication of the standard in use would not be sufficient by itself to ensure the repeatability of the test and enable the sound comparison of experimental data. As pointed out by Moylan et al. [11] and further evidenced by Phillips et al. [30], this requires a standardised reporting procedure to allow any AM user to reliably reproduce the build conditions, which is partly covered by ASTM F2971.

4.3. Specimen type and geometry-related issues

In the absence of dedicated international standards, dumbbell-shaped specimens (also called "dogbones") based on ASTM D638 [154] are very common in the literature for testing the tensile properties of FFF parts [106,141,148,155]. For example, according to the figures published by Ferreira et al. [156] in a paper regarding the FFF of PLA and PLA-matrix composite parts, ASTM D638 occurs in 8 papers out of 17, thus accounting for nearly 50% of the reviewed literature. The literature data tabulated by Goh et al. [143] also confirms the prevailing diffusion of ASTM D638, which is applied in 10 contributions out of 12. Similarly, recent statics regarding the tensile testing of composite parts printed by FFF show that, out of 158 papers in exam, ASTM D638 has been followed in 58 contributions [157]. Dumbbell-shaped specimens are also prescribed by ISO 527–2 [158], which is very similar to ASTM D638, although the non-linear portion of the stress-strain curve is treated differently in the two standards.

In spite of the overwhelming popularity of ASTM D638, there are still unsolved questions regarding the reliability of the acquired data, due to issues associated with the specimen geometry and size. ASTM D638 describes 5 different types of tensile specimens, all of which having dogbone-like shape, but with different features and proportions. In principle, different samples should be used for different testing purposes. As summarised by Fayazbakhsh et al. [142] and by Ferrell et al. [18], type I specimens are a sort of gold standard, as they are the recommended option for quasi-static tensile testing in normal conditions. Type II should be considered if failure does not occur within the narrow section of type I. Both type I and type II are relatively thin samples having a thickness smaller than 7 mm. Type III dogbones are thicker than types I and II, and should be tested when the thickness is in the range between 7 mm and 14 mm. Basically, type I and type III

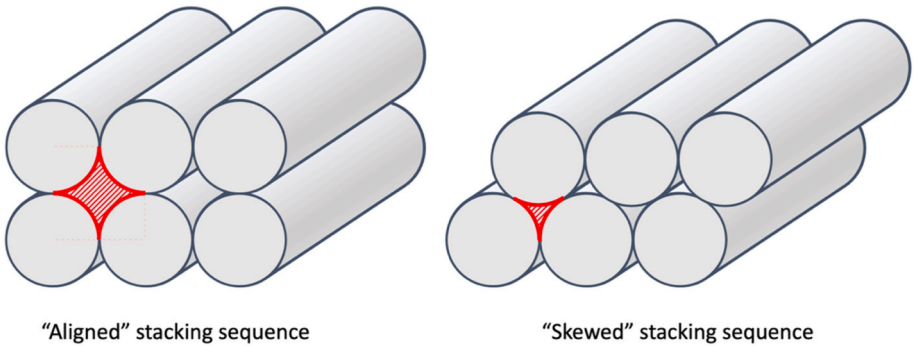

Fig. 7. Inter-raster voids (cross section highlighted in red) developed under different stacking sequences. The rasters are ideally represented as having round cross section. (For interpretation of the references to colour in this figure legend, the reader is referred to the Web version of this article.)

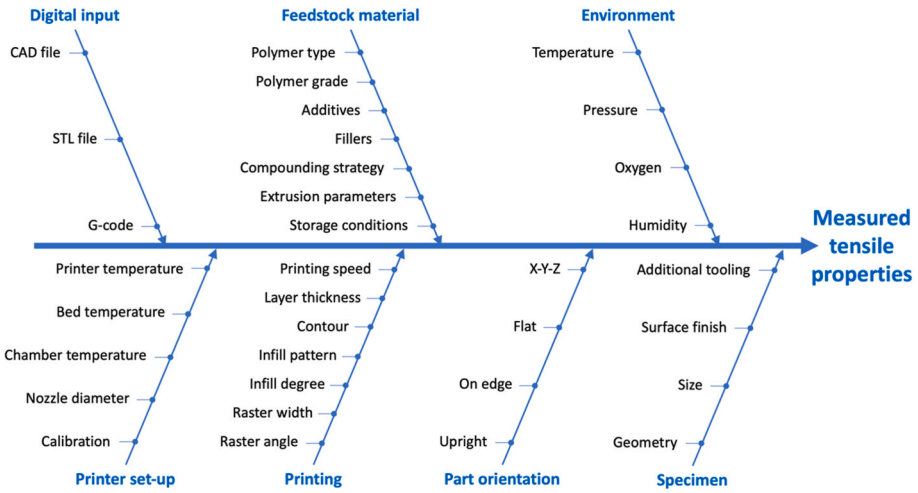

Fig. 8. Main parameters affecting the tensile properties of FFF parts.

dogbones have similar shape, but the overall size of type III is proportionally larger in order to accommodate to a larger thickness. Type IV specimens are intended for comparing non-rigid and semi-rigid materials. Type IV, which is smaller than types I, II, and III, has a very slender narrow section and relatively large grips. For this reason, the fillet in type IV specimens has a smaller radius than in type I, but the geometry also includes an outer fillet that ensures a smooth transition from the narrow section to the grips. Type I and type IV dogbones are compared in Fig. 9. Type V bars are also known as "micro-tensile" specimens, as they are similar to types I, II and III, but much smaller in size. ASTM D638 proposes type V dogbones when the material available for testing is limited, or when there are physical constraints to the size of the testing equipment, for example when a heating chamber is required [142].

Besides the general guidelines provided by the standard, the choice of the specimen type or even the decision of performing customised tests instead of standardised ones can be influenced by practical needs [10]. For instance, working with out-of-standard (mainly subsize) specimens is a forced choice owing to the limited availability of the feedstock material, especially if a new formulation is being assessed for research purposes. Smaller than prescribed samples may also be preferred for costly materials on account of the destructive nature of tensile testing [10]. When it comes to AM, another restriction to the specimen size may come from the dimension of the build volume [159], with the maximum attainable size in FFF being typically around 20 cm × 20 cm × 20 cm, unless customised equipment is used [160]. In this regard, type IV and type V dogbones are often regarded as practical options when the feedstock material or the build size are limited in FFF [48,159,161–163]. Otherwise, some authors still prefer working with type I dogbones (or other standard geometries), but scale down the specimen dimensions (examples in the contributions by Gkartzou et al. [164], Ning et al. [165,166], Uşun and Gümrük [167]).

Since ASTM D638 (as well as the similar ISO 527–2) was not originally conceived for the characterisation of AM parts, it is not clear what size and geometry should be chosen. This is a critical gap, because it has been proven that the tensile strength of FFF parts measured according to ASTM D638 is affected by the specimen type in use. For example, Torrado and Roberson [48] detected major differences in the tensile strength and elongation at break of type I, type IV, and type V dogbones. Noteworthy, the anisotropic effects were different for different geometries (even though this variability may be partly caused by the different strain rate applied when loading type V samples, as observed by Ferrell et al. [18]). Ultimately, Torrado and Roberson [48] advised that the tensile strength of type V dogbones is less dependent on the print orientation (namely, is more isotropic) than it is for type I and type IV, since similar average values were achieved by in-plane longitudinal and

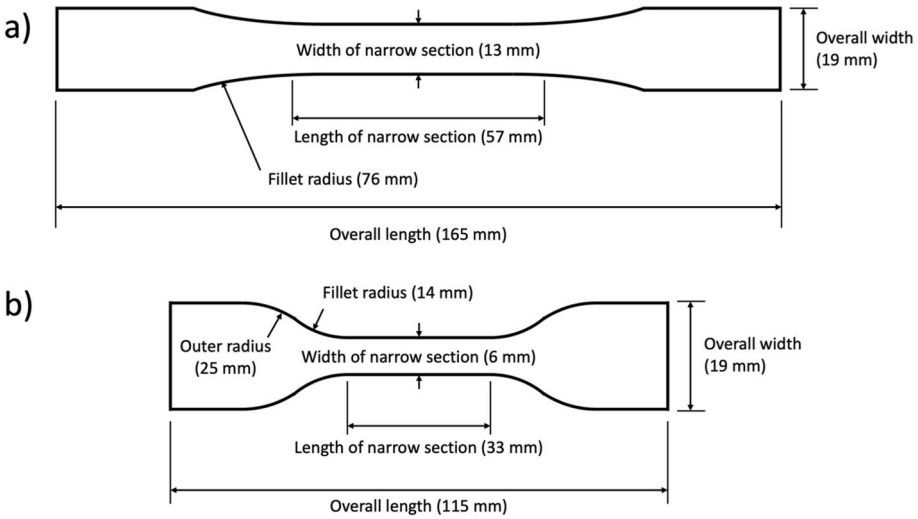

Fig. 9. Comparison between ASTM D638 type I and type IV dumbbell-like specimens (the drawing is illustrative, and only includes the nominal dimensions discussed in the text).

transverse samples, as well as by upright (vertical) samples.

Laureto and Pearce [56] compared the mechanical behaviour of type I and type IV coupons. By leveraging the distributed manufacturing capabilities of prosumer printers, 423 tensile bars were printed with 47 replicas of the same open-source do-it-yourself (DIY) delta RepRap 3-D printer. Based on the rich data acquired through this "distributed" printing campaign, Laureto and Pearce [56] concluded that type IV specimens may overestimate the ultimate tensile strength with respect to type I.

Ferrell et al. [18] rigorously compared the five types of dogbones described by ASTM D638 under identical conditions, including the strain rate. All samples were printed with the rasters being normal to the force direction, which represents the worst loading conditions for FFF parts. The greatest number of invalid test results (i.e., parts failed outside the narrow section) was observed with types IV and V, which also produced the highest variability in time to break. Ferrell et al. [18] attributed this relatively low repeatability to the smaller size of type IV and type V samples with respect to the other types, which worsened the impact of any local stress concentrations caused by the printing process. Whilst the average tensile strength was comparable for type I and type III, substantial variations were observed with the other samples, with the strength of type IV being nearly half that of type I, and with type V outperforming all other samples. According to Ferrell et al. [18], the similarity between the tensile strength of type I and type III samples suggests that this kind of geometry, having a relatively larger narrow section as compared to types II, IV, and V, may be required to achieve reliable measurement conditions.

García-Domínguez et al. [168] compared the tensile behaviour of ABS specimens printed according to ASTM D638 type I and AENOR/-UNE 116005 type 1A [169]. AENOR/UNE 116005 is a Spanish standard focused on tensile testing of polymer parts produced by AM. The sample geometry is based on ISO 527–2 and still similar to ASTM D638 type I, but with different dimensions. In particular, the narrow section of AENOR/UNE 116005 type 1A is longer (80 mm vs 57 mm) and narrower (10 mm vs 13 mm) than that of ASTM D638 type I. However, the ASTM D638 type I specimens in exam were only 3.2 mm thick, whereas the AENOR/UNE 116005 type 1A were 4 mm. Although most dogbones failed at the fillet for both specimen types, the tests performed as per AENOR/UNE 116005 were more repeatable. If confirmed also for other polymers and print set-ups, this result might be useful to direct the development of future international standards, especially if dumbbell-like geometries are to be tested for comparative purposes [168].

In spite of the popularity of dumbbell-shaped samples based on ASTM D638 and ISO 527–2, unacceptable failure occurring outside the narrow section is often observed as a consequence of the dogbone geometry being difficult to print by FFF [26,43,106,107,155,162,170–175]. In particular, the ample fillet that connects the narrow section to the grips was originally intended to reduce the stress concentration where the cross-sectional area changes in moulded specimens, or in specimens machined from sheets or plates (which are all continuous solids), but this curvature can hardly be reproduced by the rasters printed by FFF. This may result in structural defects, such as material gaps (especially if the part is contoured), abrupt termination of rasters or sudden changes in the deposition path, that are ultimately responsible for a non-axial stress state at the radii and for abnormal stress peaks, especially in relatively thin specimens [26,155,174,175]. Some examples are provided in Fig. 10. The change in cross-sectional area from the grips to the narrow section poses additional challenges when the feedstock filament is reinforced with continuous fibres that require an uninterrupted deposition path. In fact, misalignment and fibre waviness can cause substantial deviations from the theoretical tensile strength of composite specimens [176].

In order to circumvent these printing issues, the original dogbone geometry can be modified with a larger curvature radius [106,155,171]. Otherwise, many authors (examples in the contributions by Ahn et al. [26], Fernandez-Vicente et al. [99], Gebisa and Lemu [177], Montero et al. [174], Pyl et al. [178], and Somireddy et al. [98]) recommend testing straight rectangular coupons, for example as per ASTM D3039 [179], or type 2 and type 3 as per ISO 527–4 [180]. Though formally dedicated to determining the tensile properties of polymer-matrix composite materials, ASTM D3039 is often applied also to neat polymer parts printed by FFF owing to their resemblance to orthotropic laminae, as previously discussed.

Miller et al. [173] analysed the tensile behaviour of ABS specimens printed by FFF and observed that the percentage of samples meeting the criterion for acceptable failure was higher with rectangular coupons complying with ASTM D3039 over ASTM D638 type I and type IV dogbones. A comparison between ASTM D638 type I and type IV also revealed that type IV dogbones achieved on average a higher

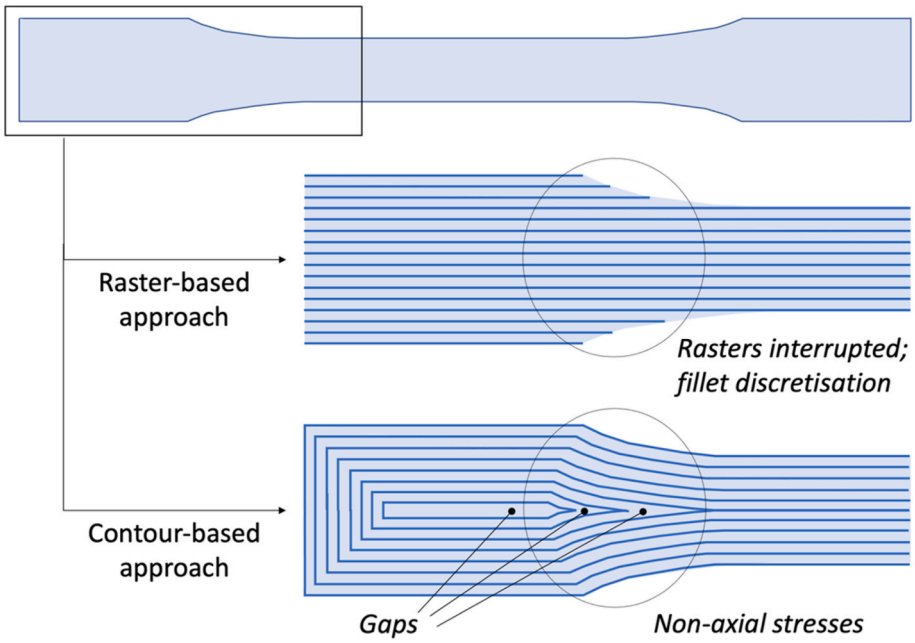

Fig. 10. Some examples of printing issues and defects observed when reproducing the curvatures of ASTM D638 dogbones in FFF parts.

compliance to the failure criterion with respect to type I. The authors identified the fillet radius as the main reason for the inconsistent failure of ASTM D638 dogbones, with the presence of the additional interior radius improving the performance (failure acceptability) of type IV dogbones as compared to type I counterparts. As already reported by Laureto and Pearce [56], Miller et al. [173] observed that the ASTM D638 type IV geometry overestimated the tensile strength. However, the data published by Miller et al. [173] also demonstrated that this geometry underestimated the elastic modulus. Opposite trends were recorded for ASTM D3039 test specimens, which led to overestimating the elastic modulus and underestimating the tensile strength. Ultimately, ASTM D638 type I performed midway between ASTM D638 type IV and ASTM D3039 both for the elastic modulus and for the strength [173].

Özen et al. [155] compared the suitability of ISO 527–2 and ASTM D3039 specimens (the latter with 3D printed end tabs) for testing the tensile behaviour of unidirectional (longitudinal) parts printed by FFF starting from a commercial glycol modified polyethylene terephthalate (PETG) filament. Since the default settings of the slicer produced weak points in the printed parts, the travel path and the slicing sequence had to be changed in order to obtain reliable results. All the geometries proved to be appropriate for measuring the elastic modulus and, for a given specimen type, the revised slicing parameters led to slightly higher average values of the elastic modulus as compared to the conventional slicing method (with the difference being comparable to the standard deviation, though). However, all samples failed prematurely, and the position of the failure was sensitive to the specimen geometry. The ASTM D3039 samples, with and without a graded transition to the end tabs, systematically failed near the tabs, which, according to ASTM D3039, sets the specimen design in question. Changing the slicing strategy was incapable of diverting the failure from near the tabs. As for the dogbone geometry, several ISO 527-2 dogbones failed in non-acceptable areas, especially at the shoulder (edge) sections. Introducing the new slicing procedure shifted the failure onset point to the narrow section and sensibly reduced the data scattering in the ultimate tensile strength. However, the transition zone between the end tabs and the narrow section of the ISO 527-2 specimens remained critical due to the local stress concentration and ultimately Özen et al. [155] advised that the curvatures in ISO-modified specimens should be increased to achieve more adequate and consistent positioning of the crack initiation point.

Table 1 maps the different kinds of samples tested in different research papers in the literature.

A concluding remark should be addressed to the location of the starting point of each layer in FFF tensile specimens. Although international standards originally conceived for other fabrication technologies fail to capture this detail, the starting point for the deposition of each layer in FFF specimens, regardless of their geometry, should be moved away from the load-bearing area (for example, the narrow section of dumbbell-like specimens) and possibly located in the grip area. Moreover, the starting point should be changed layer by layer in order to alleviate stress concentration phenomena [178,181,182].

4.4. Role of the specimen size and scale-related issues

The conflicting accounts of the role of the specimen size reported in the literature derive from the hierarchical structure of FFF parts [90], whose behaviour is dictated by the interplay between nano/-microstructure (at the sub-raster scale, including growth of crystallites and degree of crystallinity, intra-raster pores and defects, distribution of fillers and properties of the matrix-filler interface for composite parts, etc. [138]), mesostructure (at the raster scale, including raster width, raster/layer thickness, air gap, raster angle, etc. [93,95,96,183]) and macrostructure (at the part level, including, for example, the presence, the shape, the size, and the spatial arrangement of pores in lattice structures and scaffolds, or the advanced design of topologically optimised structures, etc. [184,185]).

Meza and Greer [40] thoroughly discussed the validity of the scale effect in hierarchical 3D printed parts. Traditionally, it is assumed that the properties of a material are scale-invariant, which means that objects having the same material composition and the same geometry will have the same stiffness and strength regardless of their absolute size [40]. Physically, this may be justified by the fact that, at the macroscale, the number of defects in so large that, even if the size of the object is scaled up, there is a negligible probability of producing a more severe defect [186]. Based on this principle, it can be hypothesised that, if FFF parts are bigger than the raster diameter (which is identified here as the smallest "building block" of FFF constructs), their mechanical behaviour should be scale invariant, which means that, for a given geometry, the absolute dimensions of the part should not significantly influence its mechanical properties [181,187]. This assumption is substantiated, for example, by the tensile tests performed by Ning et al. [165,166] on carbon fibre-reinforced composites. The specimens were designed as per ASTM D638 type I and printed either full-sized or scaled down by 50%. The stress-strain curves were basically overlapped for the two groups of samples, confirming that the mechanical response was insensitive to the sample size.

However, for micro-architectured materials it is generally observed that the maximum flaw size becomes smaller as the size of the object is reduced, and this correspondingly lowers the likelihood of finding a weak flaw responsible for stress concentration above the material strength. Ultimately, for nanosized constructs, the flaw size becomes comparable to the characteristic length scale of the material, and failure is governed by material heterogeneities, like grain boundaries and junctions [40]. In other words, the size invariancy does not hold true anymore when the characteristic size of the object's architecture approaches the characteristic length scale of the material structure, as it happens in natural constructs like nacre [40]. At that point, mechanical properties cease to be size invariant and, in particular, the strength increases when the architecture becomes smaller (or when only a small volume of the architecture is mechanically loaded) [188]. Size effects have been reported for a broad range of materials and constructs, from concrete structures to fibre composites, from metal alloys to solid polymers [186,188–190]. This also includes extruded filaments, as long as evidence exists in the literature that, for a given material, the smaller

Table 1
Standardised tensile sample geometries compared in the literature. Abbreviations: PLA = poly(lactic acid); ABS = acrylonitrile-butadiene-styrene; CF-ABS = chopped fibre-reinforced ABS; PETG = glycol modified polyethylene terephthalate.

Reference	Material	ASTM D638					ISO 527-2	AENOR/UNE 116005	ASTM D3039
		Type I	Type II	Type III	Type IV	Type V		Type 1A	
Ferrell et al. [18]	CF-ABS	X	X	X	X	X			
García-Domínguez et al. [168]	ABS	X						X	
Laureto and Pearce [56]	PLA	X			X				
Miller et al. [173]	ABS	X			X				X
Özen et al. [155]	PETG						X		X
Present paper	PLA	X							X
Torrado and Roberson [48]	ABS	X			X	X			

the diameter of the extruded filament, the higher the tensile strength [191]. For example, Baucom et al. [192] mixed a liquid crystalline polymer matrix with vapor-grown carbon nanofibers having diameters in the 100–200 nm range, and extruded several filaments between 0.5 and 2 mm in diameter. Due to the hierarchical structure of the filaments, whose diameter was comparable to that of the carbon nanofibers, there was a significant improvement in mechanical strength as the filament diameter was decreased.

In principle, this reasoning can be extended to the individual rasters in FFF structures, wherein intra-raster microstructural defects are expected to become smaller as the raster diameter decreases. Moreover, as proved by Górecka et al. [193] for 3D printed poly(ε-caprolactone) (PCL) rasters, the smaller diameter of the extrudate and the increased shear rate experienced by the melt while flowing through a smaller print nozzle may promote molecular orientation, facilitate supramolecular interactions and, for semi-crystalline polymers, induce a higher content of crystalline phase, which all contribute to the strength of the raster in the flow direction.

However, the raster diameter in FFF cannot be reduced freely, as its minimum value is constrained by the printing parameters and especially by the print nozzle, whose diameter in commercial printers is typically 400 μm [194]. Although smaller diameters are being considered for research purposes [195], the smallest value is still around 180 μm [193]. Moreover, due to the die-swelling effect (namely, the recovery of the elastic deformation at the exit of the nozzle), the actual size of the raster is larger than the nominal outlet diameter, with the scaling factor being approximately 1.2 [196]. As previously mentioned, the raster tends to flatten down on the base platform (or on the previous layers), which further increases the raster width as compared to the nozzle diameter. All this poses a physical barrier to the activation of scale effects through the miniaturisation of the rasters as the "building blocks" of FFF structures. On the other hand, it should be emphasised that FFF parts are not made up of individual rasters, since rasters should fuse together into a solid object. In this regard, working with larger rasters would be beneficial, because, for a given material, larger rasters cool down more slowly, and this improves the bonding quality [196].

Whilst it is not possible to have rasters smaller than 180–200 μm, it is predicted that, for a given raster diameter, the effect of the intra-raster defects will be less critical for larger parts. This is consistent, for example, with the results reported by Wendt et al. [181] that, upon testing PLA monolayer samples under tensile loading, recommended using coupons with a high width-to-thickness ratio, where the thickness of a monolayer nominally corresponds to the raster size. It was concluded that the higher the width-to-thickness ratio, the lower the effect of potential defects within single rasters.

Tekinalp et al. [21] reported lower-than-expected values of the tensile strength and Young's modulus for ASTM D638 Type V dogbones containing 40 wt% of short carbon fibres in an ABS matrix. These samples were very difficult to print due to repeated nozzle clogging, and the build was ultimately interrupted after printing just a few layers corresponding to a thickness of 0.6 mm against the targeted 3.8 mm. In addition to the microstructural defectiveness, Tekinalp et al. [21] attributed the poor mechanical performance to the limited thickness of these samples, which likely caused edge effects and poor packing density. As observed by Rankouhi et al. [175], increasing the number of layers can help mitigate the consequence of stress concentration, as each new layer contributes to filling the gaps in the previous layer. Although not strictly related to the size effect, it is also worth noting that, as pointed out by Tekinalp et al. [21], a difference in thickness may impact the instrument sensitivity during measurement.

In addition to the presence of microstructural defects, the role of the sample size may also be influenced by mesostructural features like the inter-raster joints and air gaps. Interestingly, for a given set of printing parameters, the size of these mesostructural features is constant, regardless of the overall size of the part. This means that the size effect is violated, in that the flaw size does not change with the object's size. As previously seen for intra-rasters defects, the effect of mesostructural features is thus expected to lessen as the object's size increases. This all suggests that increasing the part's size should enhance the mechanical strength. However, more rasters and more layers will be needed to complete a larger part, which implies that the number of flaws will increase if the object's size increases. Finally, scaling up an FFF object has two opposing effects, as it mitigates the consequence of individual defects, but also multiplies the number of defects. Which one of these competing effects is prevailing should be determined on a case-by-case basis.

For example, as explained by Torrado and Roberson [48], the small size of type V dogbones as per ASTM 638 may be problematic when testing FFF parts in that the cross-sectional dimensions of the narrow section (indicatively: width of 3.18 mm, thickness of less than 4 mm) are close to a factor of ten compared to the raster size (indicatively: width of 0.4 mm, thickness of 0.27 mm), and this increases the effect of inter-raster air gaps. Similarly, Xu et al. [182] observed a progressive decline in tensile strength and Young's modulus as the size of ASTM D638 (presumably, type I) dogbones was reduced from 100% to 50% and finally to 30%. The poorer performance of the downscaled samples was attributed to several causes. However, the main factor was the structural weakness of the first deposited layer (which was supposed to be comparable for all samples, irrespective of their size), as it severely impacted the overall behaviour of smaller, and hence thinner, specimens. Drummer et al. [197] also pointed out that, if the raster size is the same, building larger parts requires more layers and more rasters within each layer. Since the extrudate is still very hot when being deposited, the pre-existing rasters are re-heated several times, and this may promote the crystallisation of semi-crystalline polymers such as PLA, thus increasing the stiffness (Young's modulus) of larger parts. However, as previously mentioned, the increased crystallinity may also hinder the inter-raster welding process [89]. Besides these material-related factors, decreasing the size of the part may engender hardware-related hurdles, since it has been argued that, as the size of the part decreases in the millimetre and sub-millimetre range, physical limitations such as the tolerance of the belt that moves the printhead on the gantry and the step error of the motor become more apparent, and this undermines the reliability and accuracy of the printed structure [198]. Besides the tensile behaviour, scaling effects, whereby the mechanical properties of FFF constructs become worse as the part's size is decreased, have also been reported for flexural and compressive properties. Aziz et al. [199] noticed that, apart from minor differences, the flexural and compressive behaviour of larger parts could be qualitatively predicted from the stress-strain curves of geometrically similar smaller parts. However, both the flexural strength and the compressive strength were lower for smaller parts, which was attributed to the layer-wise surface roughness and to the microstructural porosity, whose size was the same for all specimens, having a stronger influence on smaller specimens. This scale-related effect was difficult to predict, though, since no sound correlations were observed between strength (either flexural or compressive) and size, with the largest samples outperforming the smallest ones by 17.9% with respect to the flexural strength, and by 18.2% with respect to the compressive strength, when the linear dimensions were scaled by a factor of 4. The scale-related effects became even more relevant when body-centred cubic lattices were compared, as the compressive strength increased by 60% when the linear dimensions of the lattices were increased by a factor of 4. Conversely, Pagano et al. [185] did not record any changes in compressive strength when the height of PLA scaffolds was increased from 6 mm (15 layers) to 24 mm (60 layers), which led to the conclusion that the compressive strength would be an intrinsic property of the structure. Meanwhile, the compressive stiffness sensibly increased from around 400 MPa to nearly 700 MPa. However, it should be mentioned that, whilst in the research conducted by Aziz et al. [199] all testing parameters were geometrically scaled, in the paper by Pagano et al. [185] only the height of the scaffolds was changed, which may have contributed to the different trends

observed for the compressive stiffness and strength.

Based on the limited data available so far, it is presently unknown whether a size threshold exists, below which FFF parts suffer a reduction in strength as their size becomes smaller. The existence of a size threshold was actually demonstrated with PolyJet parts [200]. However, PolyJet (which belongs to the material jetting family, "MJT", according to ISO/ASTM 52900) and FFF are different AM technologies, and therefore further research is certainly needed to understand if this finding regarding the existence of a size threshold can be transferred to FFF. Also, reaching any sound conclusions regarding the scaling effects in FFF becomes baffling on account of the mutually opposed observations published in the literature. For example, the trends described by Vălean et al. [201] clearly point towards the existence of an inverse relationship between dimensions and mechanical properties (specifically, Young's modulus and tensile strength). In the experiment conducted by Vălean et al. [201], ISO 527–1 [202] dogbones were printed with increasing thickness values, ranging from 1.25 mm to 8.00 mm, while keeping the in-plane dimensions unchanged. All samples were unidirectional, with the rasters being parallel to the load direction. Both the Young's modulus and the tensile strength progressively decreased for increasing thickness values. According to Vălean et al. [201], the number of defects increased as the sample size increased, and this caused the specimens to fail under lower applied loads. Decker et al. [198] demonstrated that the failure mode of PLA tensile specimens (not complying with existing standards) changed from brittle to ductile when the cross-sectional area was reduced from 10 mm × 10 mm to 2 mm × 2 mm. The different behaviour was tentatively attributed to the different thermal history, with the smaller samples experiencing a shorter cycle time and thus achieving a better inter-layer adhesion. A similar hypothesis was also formulated by Guessasma et al. [203], who measured a progressive decline in the compressive strength of ABS blocks (cubes) when the edge length was increased from 5 mm to 40, with a sudden drop occurring from 20 mm (64.5 ± 0.1 MPa) to 40 mm (49.3 ± 2.5 MPa). The longer distance travelled by the extrudate and hence the longer time elapsed between the deposition of subsequent layers were held responsible for a lack of cohesive bonding in the larger cubes.

Besides the role of raster-raster interfaces and defects, another mesoscale variable that affects size-related phenomena is the presence of a contour. Kung et al. [204] noticed that the tensile strength of PLA dogbones printed according to ASTM D638-2a sensibly increased when the sample size was scaled down to 75%. Meanwhile, the data scattering became smaller, thus suggesting that the mechanical strength of the smaller samples was more consistent and reliable than that of the full-size samples. Kung et al. [204] argued that the perimeter (if present) plays an important role in taking up a fraction of the applied tensile load. Since the raster diameter was the same for all samples, Kung et al. [204] attributed the higher strength of the smaller samples to the perimeter area-to-infill area ratio being higher in these samples than in the full-size benchmarks. Similar conclusions were drawn by Elmrabet and Siegkas [108], who compared the tensile properties of PLA specimens printed according to ISO 37 (with ISO 37 describing dumbbell-like specimens for tensile testing of rubber, vulcanized or thermoplastic materials [205]; tested dimensions of the narrow section: 25 mm long, 2 mm thick) and according to ISO 527 type 1A and 1B with different infill degrees, and observed that the smaller ISO 37 PLA specimens at 20% infill behaved similarly to larger ISO 527 specimens (both types) at 100% infill. This difference was attributed to the perimeter of the smaller cross section of ISO 37 specimens being proportionally larger than that of the larger cross section of ISO 527 specimens, and hence producing a higher overall density, closer to 100%. The most detrimental condition was reported for larger parts compliant with ISO 527 printed with a low infill degree (i.e., 20% and 60%), as the infill gaps would result in large voids promoting the initiation and propagation of cracks. García-Domínguez et al. [168] also observed that the contour becomes critical when the rasters in the narrow section are normal to the loading direction. In this case, the contour, being parallel to the loading direction, carries most of the load and contributes to preserve the structural integrity of the part.

Lastly, it is worth noting that different properties may be differently affected by defects and structural features. For example, the research by Fayazbakhsh et al. [142] demonstrated that the presence of missing rasters in PLA dogbones as per ASTM D638 type I sensibly reduces the tensile strength, but has a minor effect on the Young's modulus. As for the failure at break, the consequence of missing rasters cannot be generalised, as it depends on the specific nature of the defect. Typically, missing rasters transverse to the loading direction largely reduce the deformation at break. Conversely, although this may be counterintuitive, missing rasters parallel to the loading direction may increase the deformation at break through improved material redistribution mechanisms [142].

Table 2 provides a summary of the main trends reported in the literature regarding the effect of the specimen size on the measured mechanical properties. Though the focus is on the tensile behaviour, for the sake of completeness information is also provided regarding other mechanical properties.

4.5. Single raster- and layer-based approaches to tensile testing of FFF parts

Starting from the assumption that conventional test specimens are not suitable for AM, Wendt et al. [181,187] outlined a new methodology based on monolayer specimens, which are made from only one layer of material. The underpinning philosophy is that testing should start from the simplest elements, and the single layer is "the simplest unit of a complex multilayer part" [187]. In order to demonstrate the effectiveness of the monolayer design and testing procedure, Wendt et al. [187] considered flat monolayer coupons printed by FFF starting from a commercial PLA filament. The specimens were basic rectangles having longitudinal rasters in the load-bearing region. However, the same geometry was built according to different toolpaths, including a zig-zag parallel route, a circular route starting in the centre (outward), a circular route starting on the perimeter (inward), and a circular route inward having an external starting point. Some trajectory strategies for tensile specimens are exemplified in Fig. 11 [181]. In spite of the conceptual simplicity of the targeted rectangular geometry, the samples were often faulty, and printing adequate coupons for tensile testing required additional design adjustments [187]. A small rectangular hole had to be introduced in the centre of the coupon to reduce warping and compensate for over-feeding. The tensile strength and the modulus of elasticity of the corrected samples were highly repeatable and comparable to those of the feedstock filament. However, the nominal value of the cross-sectional area of the coupons had to be used in calculating these values, due to the extremely irregular and undulated profile of the specimens impeding a straightforward measurement of the real area [187]. In a subsequent contribution, Wendt et al. [181] also considered a single-layer dumbbell-shaped geometry (as per ISO 3167 type A [206]). Interestingly, only one specimen out of five failed outside the narrow section [181].

Some studies in the literature investigate the tensile properties of single rasters as the smallest building blocks of FFF structures. For example, Bellini and Güçeri [207] designed a special cardboard frame to clamp and test the single rasters printed with a commercial ABS filament. The results collected from these tensile tests on single rasters served as input to calculate the stiffness matrix describing the mechanical behaviour of a printed part according to the CLT. A similar tensile test conducted on the original feedstock filament revealed that the tensile strength and Young's modulus had not been changed by the printing process. However, the deformation at break of the single rasters was smaller than that of the filament, with the difference being attributed to the molecular orientation phenomena occurring in the print nozzle [207].

Paying attention to the behaviour of individual rasters is justified by the functioning mechanism of FFF, where individual layers are

Table 2
Contrasting effects of the specimen size on the measured mechanical properties of FFF constructs as reported in the literature. Due to space constraints, the main reasons are just briefly mentioned here, whilst further detail can be found in the main text and in the referenced papers. Abbreviations: PLA = poly(lactic acid); ABS = acrylonitrile-butadiene-styrene.

Reference	Material	Test	Effect of size	Reason
Ning et al. [165]	ABS + 5 wt % chopped carbon fibres	Tensile	None	
Ning et al. [166]	ABS + 5 wt % chopped carbon fibres ABS + 5 wt% graphite	Tensile	None	
Aziz et al. [199]	PLA	Flexural; compressive; compressive on lattices	Larger is better	Layer-induced surface roughness and intra-raster porosity less impactful on larger parts
Decker et al. [198]	PLA+ (PLA + 2% calcium carbonate)	Tensile	Larger is better	Hardware-related errors less impactful on larger parts
Drummer et al. [197]	PLA + 2.5 wt% tricalcium phosphate	Tensile	Larger is better	Repeated heating promotes crystallisation in larger parts
Pagano et al. [185]	PLA	Compressive on lattices	Larger is better	While the strength is constant, the compressive stiffness increases with the lattice's height
Present paper	*PLA*	*Tensile*	*Larger is better depending on raster angle*	*Opposing effect of longer exposure to high temperature and increased number of defects in larger parts*
Rankouhi et al. [175]	ABS	Tensile	Larger is better	More layers and thicker mitigate residual stresses
Tekinalp et al. [21]	ABS + 40 wt % short carbon fibres	Tensile	Larger is better	Edge effects and poor packing density in thinner samples
Torrado and Roberson [48]	ABS	Tensile	Larger is better	Narrow section comparable to raster size in small samples
Wendt et al. [181]	PLA	Tensile	Larger is better	Intra-raster defects and surface waviness less impactful on larger parts
Xu et al. [182]	PLA	Tensile	Larger is better	Deviations caused by first layer more impactful on smaller samples
Decker et al. [198]	PLA+ (PLA + 2% calcium carbonate)	Tensile	Smaller is better	Shorter cycle time improves inter-layer adhesion in smaller parts
Elmrabet and Siegkas [108]	PLA	Tensile	Smaller is better	Higher ratio between perimeter area and infill area in smaller samples
Guessasma et al. [203]	ABS	Compressive	Smaller is better	Shorter cycle time improves inter-layer adhesion in smaller parts
Kung et al. [204]	PLA	Tensile	Smaller is better	Higher ratio between perimeter area and infill area in smaller samples
Vălean et al. [201]	PLA	Tensile	Smaller is better	More defects in larger parts

comprised of rasters. Moreover, in a larger context, taking into account the fact that standardised procedures are required in all technologies, the raster-based approach to mechanical testing could be extended to other track-based AM process, such as electron beam melting (EBM) or selective laser melting (SLM) (both of them in the PBF family as per ISO/ASTM 52900) However, this raster-based testing would be unfeasible for those techniques that add one layer at a time, like digital light processing (DLP, in the VPP family) or laminated object manufacturing (LOM, in the sheet lamination, SHL, family) [181].

Sometimes tensile tests are repeated on the feedstock filament, on a single "structural unit" that can be either a single raster (for example, in the contribution by Stoof and Pickering [208]) or a single layer (for example, in the contribution by Berretta et al. [209]), and then again on multi-layered specimens. This procedure may be very useful to track down the effect of printing at different stages of the part's fabrication. However, despite the conceptual relevance of these out-of-standard tests on single rasters and layers, their repeatability and transferability to other materials may be problematic, even if the specific testing protocol is described in detail.

4.6. Other testing variables

As seen before, the adoption of specimens having appropriate size and geometry is key for achieving sound tensile testing results. However, other relevant variables should also be taken into consideration. Since polymers have a viscoelastic behaviour, their response to an applied load depends on the temperature and on the strain rate [210,211]. Whilst tensile tests are routinely performed at room temperature unless differently stated, the effect of the strain rate remains largely unexplored for FFF parts. Vidakis et al. [212] compared the strain rate sensitivity of PLA, ABS, PETG, polyamide 6 (PA6), and polypropylene (PP) ASTM D638 type V FFF specimens tested under 5 different loading rates spanning from 10 to 100 mm/min. Generally speaking, the yield strength and the tensile strength slightly increased with higher loading rates, due to strain hardening phenomena. This is consistent with the trends observed, for example, by Tymrak et al. [43] for PLA parts, and by Rodriguez et al. [213] for ABS parts. Vidakis et al. [212] also noticed that the failure mechanism and the strain rate sensitivity were material-dependent. The failure mechanism of PLA, ABS, PETG and PP gradually changed from brittle fracture at low loading rates to ductile fracture at high loading rates. Conversely, PA6 experienced a prevalent plastic deformation leading to ductile fracture over the whole range of loading rates under exam. Interestingly, as discussed by Vidakis et al. [212], ASTM D638 recommends using either 10 or 100 mm/min as the speed of testing for type V specimens, with 10 mm/min being the most popular option in industrial applications. This means that different results should be expected for FFF parts tested under different loading rates, even if the testing parameters are formally chosen "according to the standard".

In the research conducted by Ferrell et al. [18], the tensile strength of ASTM D638 type V dogbones largely exceeded the values recorded for

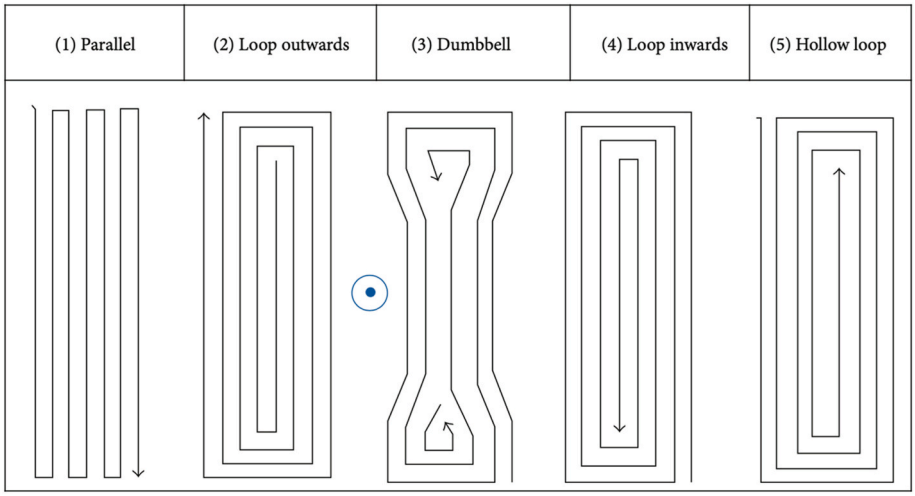

Fig. 11. Trajectory strategies for building tensile specimens investigated by Wendt et al. [167]. The blue dot points towards the build (growth) direction (*Reproduced from Wendt* et al. [181] *under the Creative Commons Attribution License*). (For interpretation of the references to colour in this figure legend, the reader is referred to the Web version of this article.)

all other ASTM D638 dogbones printed under the same conditions when the tests were conducted under a loading rate of 1 mm/min. At the same time, these specimens suffered a high rate of invalid failure. Ferrell et al. [18] argued that the anomalous behaviour might be due to the loading rate being too high for type V dogbones. As a matter of fact, repeating the test under a lower strain rate (0.2 mm/min) reduced the average tensile strength of type V dogbones to a value closer to that observed for the other types. This confirms the importance of adjusting the strain rate to the specific specimen type in use [18]. Moreover, Wendt et al. [181] pointed out that, even for a given specimen type, the most appropriate loading rate may be different for measuring the tensile strength and the Young's modulus.

Another point that is often overlooked in the literature is the effectiveness of clamping on FFF tensile specimens [178]. In this regard, Özen et al. [155] recommended the use of tabs to provide an adequate clamping. As stated by Wendt et al. [181], additional measures may be necessary, such as working with file-teeth grips, because the real contact area of FFF specimens with the grips is reduced with respect to the nominal value due to the raster-induced surface waviness.

5. Case study: determination of the tensile properties of PLA parts

5.1. Objectives

From the analysis of the literature above, it is well understood that the tensile properties of FFF components vary dramatically based on different processing parameters. Since there are currently no designated standards for mechanical testing of FFF parts, it has become common practice to adopt existing test standards to analyse the mechanical properties of the components processed by FFF. However, test methods set out within conventional standards inadequately account for the inherent structural variability and complexity manifested in FFF components. In particular, varying specimen size and geometry requirements across different standards can lead to deviations in the measured values, making it difficult to draw sound conclusions regarding the mechanical performance of FFF parts.

This case study quantitatively assesses the importance of standardisation in the tensile testing of AM parts. To this aim, tensile test specimens were fabricated via the FFF technique, using PLA as the feedstock material. Two of the recommended standards for tensile testing of FFF parts, namely ASTM D638 Type I and ASTM D3039, were employed in order to elucidate the effect of the specimen geometry. Moreover, the effect of the specimen size was also investigated by reducing the size of ASTM D3039 bars. All samples were printed flat on the base platform, either with a 0° or a 90° raster angle. In addition, the tensile properties of compression moulded PLA specimens were also tested to provide a term of comparison for the FFF parts.

While the measurement of the tensile properties of PLA parts has been proposed in the literature several times [214–216], this case study highlights the anisotropic effects induced by the raster angle and statistically demonstrates that the measured tensile properties are different when the FFF parts are printed with different geometry and size, even if all the specimens nominally comply with the standards. Moreover, for the first time, the experimental findings suggest that a correlation exists between raster angle and specimen size.

5.2. Materials and methods

5.2.1. Materials

Commercial grade PLA pellets were purchased from NatureWorks LLC (Minnetonka, MN, USA) with the trade name of Ingeo™ 3D850, which is a grade developed for manufacturing 3D printing monofilaments. According to the technical data sheet [217], this material has a melt flow rate of 7–9 g/10 min, a specific gravity of 1.24 g/cm^3, a glass transition temperature of 55–60 °C, and a melt temperature of 165–180 °C.

5.2.2. Fabrication of PLA filaments

Before processing, PLA pellets were dried overnight at 70 °C. Dried PLA pellets were then melt-extruded in a co-rotating twin-screw extruder (Prism EuroLab 16 TSE, ThermoFisher Scientific, Waltham, MA, USA) to produce PLA filaments. The temperatures of the ten heating zones were set at 20, 20, 70, 100, 160, 170, 180, 190, 205, and 205 °C, respectively. The screw rotation speed was set at a constant 200 rpm. After extrusion, the 1.75(±0.05) mm filaments were cooled and collected on a conveyor belt before being rolled onto a spool.

5.2.3. FFF printing

3D printed PLA specimens were produced via an FFF printer (Raise3D Pro 2, Raise 3D Technologies, Irvine, CA, USA) using the previously custom-made filaments. To demonstrate that print orientation has a direct influence on the mechanical properties of the printed parts, the tensile specimens were printed at two different raster angles as exemplified in Fig. 12, namely (i) 0° (parallel to the loading direction), and (ii) 90° (perpendicular to the loading direction).

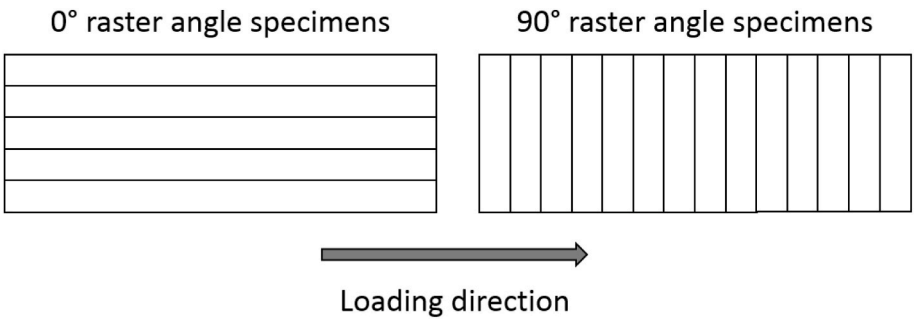

Fig. 12. Raster angles used in the FFF tensile specimens.

Each specimen was printed individually in the same location on the base platform to minimise the variables in play. Other printing parameters such as infill density, layer thickness, print speed, and print temperature were kept constant. The details of these printing parameters are listed in Table 3.

Two different specimen geometries were considered for comparative purposes. To accomplish this, samples were printed according to ASTM D638 type I, as illustrated in Fig. 9(a) using the raster-based approach (as shown in Fig. 10), and according to ASTM D3039, as shown in Fig. 13. According to ASTM D3039, test specimens are rectangular in shape with a constant cross-sectional area. Although specific dimensions are not detailed for the D3039 test geometry, it is required that the minimum length of the specimen to be the sum of the grip length, twice the width, and the gauge length.

The choice of the dimensions for the ASTM D3039 rectangular bars (i.e., width: 25 mm × length: 229 mm × thickness: 3 mm; "Large" specimens hereafter) was based on the contribution by Miller et [173] that reported a 95% compliance with ASTM D3039 failure acceptance criteria. In order to explore the role of the specimen size, a second set of specimens was printed according to ASTM D3039 with smaller dimensions (i.e., width: 22 mm × length: 200 mm × thickness: 3 mm; "Small" specimens hereafter), which also correspond to the largest size attainable with the hot press in use. As a result, the dimensions of the Small specimens were a factor of 0.9 of those of the Large specimens.

5.2.4. Compression moulding

Compression moulded PLA specimens complying with ASTM D3039 were manufactured with a hydraulic hot press machine with a maximum working pressure of 150 kPa and two heated platens measuring 230 mm × 230 mm. The mould to produce the ASTM D3039 tensile bars was customised from a steel plate. Laser cutting was used to form rectangular cavities according to the targeted size of the tensile bars. The custom-made extruded PLA filaments were pelletised and loaded into the cavities for compression moulding at 190 °C. The samples were produced from the same filaments used for printing, and not from the original pellets, in order to enable a more direct comparison between the two manufacturing processes. As mentioned before, due to the size limitation of the platens of the hot press, only Small specimens could be fabricated.

Table 3
FFF Printing parameters.

Printing parameter	Set value
Infill density (%)	100
Infill flowrate (%)	90
First layer thickness (mm)	0.3
Layer thickness (mm)	0.2
First layer print speed (mm/s)	30
Print speed (mm/s)	70
Print temperature (°C)	230
Bed temperature (°C)	60
Build orientation	flat on x-y plane
Print direction	parallel to the x-axis
Nozzle diameter (mm)	0.4

5.2.5. Tensile testing

Table 4 summarises the tensile test specimen configurations and the experimental factors considered in this study. Five specimens were tested for each configuration, with each specimen being pre-dried at 40 °C overnight before testing. The tensile tests were conducted at room temperature on a universal testing machine (5900 R, Instron, Norwood, MA, USA), with a load cell of 30 kN. The specimens were loaded at 5 mm/min and at 2 mm/min as per the ASTM D638 and ASTM D3039 standards, respectively, until fracture. An extensometer was not used due to the brittle nature of the samples that, in spite of some local necking occasionally observed within individual rasters of the 0° raster angle specimens, resulted in a sudden failure. The stress-strain curves were elaborated to obtain the elongation at break (EAB), the ultimate tensile strength (UTS), and the elastic modulus (EM). The UTS (which also corresponds to the "tensile strength" owing to the brittle behaviour of the PLA specimens) was determined from the maximum load at break, whilst the EM was calculated from the slope of the linear elastic region of the stress-strain curves.

5.2.6. Statistical analysis

A two-way analysis of variance (ANOVA) was performed to validate the statistical relevance of the effect of the raster angle and the size on the mechanical properties of the printed specimens using SPSS software (IBM, Armonk, NY, USA). The p-value associated with the analysis was correlated to a significance level of 0.05.

5.2.7. X-ray diffraction

A Bruker D8 Advance A25 X-ray Diffractometer operating under CuKα radiation (40 kV, 40 mA) equipped with a Lynx Eye XE-T detector was employed to obtain the X-ray diffraction (XRD) patterns of the specimens complying with ASTM D3039 (one specimen per set). The samples were scanned over the 5°–85° 2θ range, with a step size of 0.02° and a count time of 1.6 s per step, and were spun at 15 RPM (rotations per minute) during data collection.

5.2.8. Micro-computed tomography (μCT) analysis

A Zeiss Xradia 515 Versa X-ray microscope (Zeiss, Oberkochen, Germany) equipped with an FPX detector was employed to evaluate the internal porosity of the 3D printed and compression moulded specimens. All scans were taken at a voltage of 40 keV with a power of 3 W, exposure time of 2 s, and effective pixel size of 17.63 μm. 801 projections were taken from a full 360° rotation. The distance of the rotation axis to the source and detector was set at −34.06 mm and 254.98 mm, respectively. Subsequently, porosity measurements were performed with Avizo software (Thermo Fisher Scientific, WA, MA, USA). Auto-thresholding was applied to separate materials from voids, followed by the adoption of volume fraction module to compute the volume fraction of voids in each specimen.

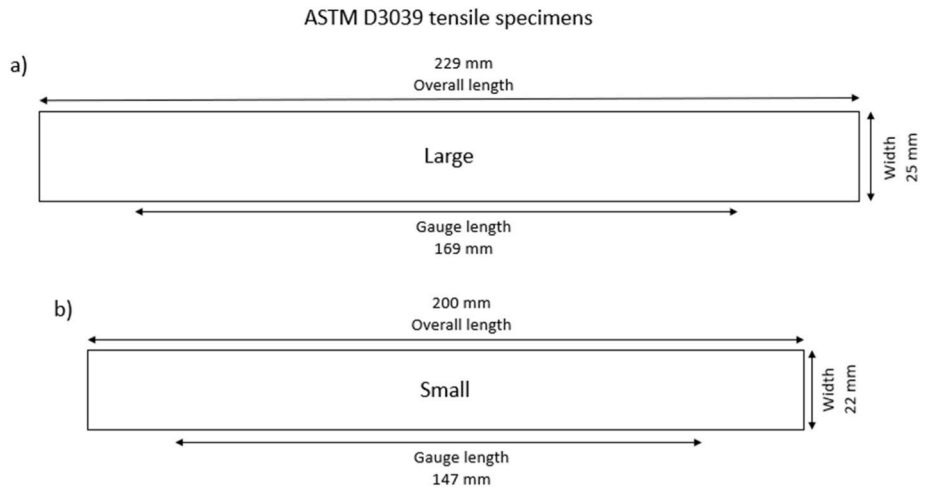

Fig. 13. ASTM D3039 tensile test geometry and sizes: (a) Large specimens; and (b) Small specimens.

5.3. Results and discussion

5.3.1. Effect of the specimen geometry

In this study, dumbbell-like specimens were initially printed as per ASTM D638 Type I, which is often recommended in the literature for tensile testing of FFF parts [29]. According to this standard, an important criterion for the measurements to be valid is that the specimens must break within the length of the narrow section. As shown in Fig. 14, none of the 0° raster angle specimens and only one of the 90° raster angle specimens satisfied this failure acceptance criterion. Nine specimens out of ten failed at a point near the grips around the fillets, which suggests that dumbbell-like specimens are inadequate to quantify the tensile properties of the FFF parts in exam. As a matter of fact, this has been considered a primary failure mode for many FFF printed objects [199], due to stress concentration developed from the abrupt shape transition of the dog-bone geometry and the presence of voids in the gauge section.

Although strictly speaking only one 90° raster angle specimen should be considered for valid test results, all stress-strain curves were elaborated, and the UTS, EAB, and EM are plotted in the bar graphs in Fig. 15. Although these values are not meant to be acceptable according to the standard (average values should be calculated over five valid specimens per configuration, as also discussed by Miller et al. [173]), they provide a qualitative understanding of the behaviour of parts printed with different raster angles, with the 0° raster angle specimens performing better than the 90° raster angle counterparts in respect of all the tested properties.

Taking into account the extremely limited number of specimens meeting the failure acceptance criterion of ASTM D638, the specimen geometry was simplified to a straight rectangle compliant with the ASTM D3039 standard, which is also frequently recommended in the literature for tensile testing of FFF parts [173], and only this geometry was considered for additional investigation.

5.3.2. Effect of the raster angle and the specimen size

All rectangular samples, both Large and Small, failed consistently with the failure acceptance criterion as per ASTM D3039, which allowed the results for different raster angles and for different sizes to be statistically compared. The average values and the standard deviations of the tensile properties are presented in Fig. 16.

According to the charts in Fig. 16, the raster angle clearly exerts a significant influence on the mechanical properties of the printed parts. All 0° raster angle specimens exhibited higher UTS, EAB, and EM values as compared to the 90° raster angle specimens, regardless of the specimen size. Conversely, the effect of the specimen size on the tensile properties appears to be less obvious, since an opposing trend can be observed for the UTS and EAB at different raster angles. Whilst the UTS and EAB of the Large_0 specimens are about 10% and 14% higher, respectively, than those of the Small_0 specimens, in contrast, the UTS and EAB of the Large_90 specimens are around 11% and 13% lower, respectively, than those of the Small_90 specimens. According to these mutually opposing trends, it may be hypothesised that the effect of the specimen size may be dependent on the raster angle.

The interplay between size and raster angle was validated via

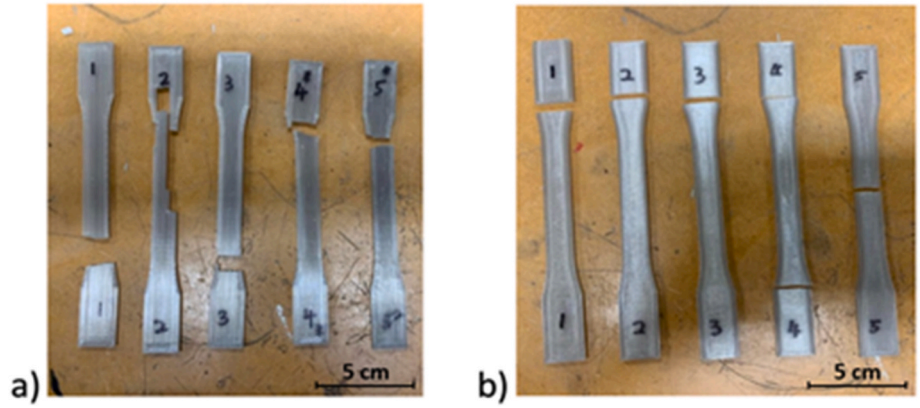

Fig. 14. Photographs of ASTM D638 Type I tensile specimens after tensile testing: (a) 0° raster angle, and (b) 90° raster angle. Overall length of each specimen before failure: 165 mm.

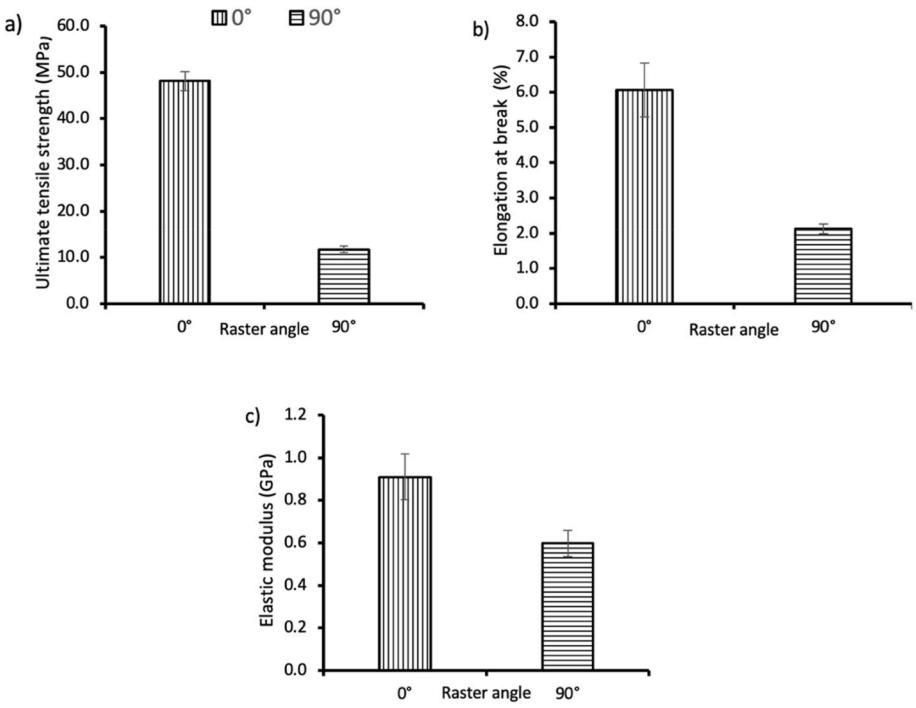

Fig. 15. Bar charts of the average tensile properties and standard deviations of the ASTM D638 Type I specimens taken from 5 specimens (though broken outside the narrow section, as explained in the text): (a) ultimate tensile strength, UTS; (b) elongation at break, EAB; and (c) elastic modulus, EM.

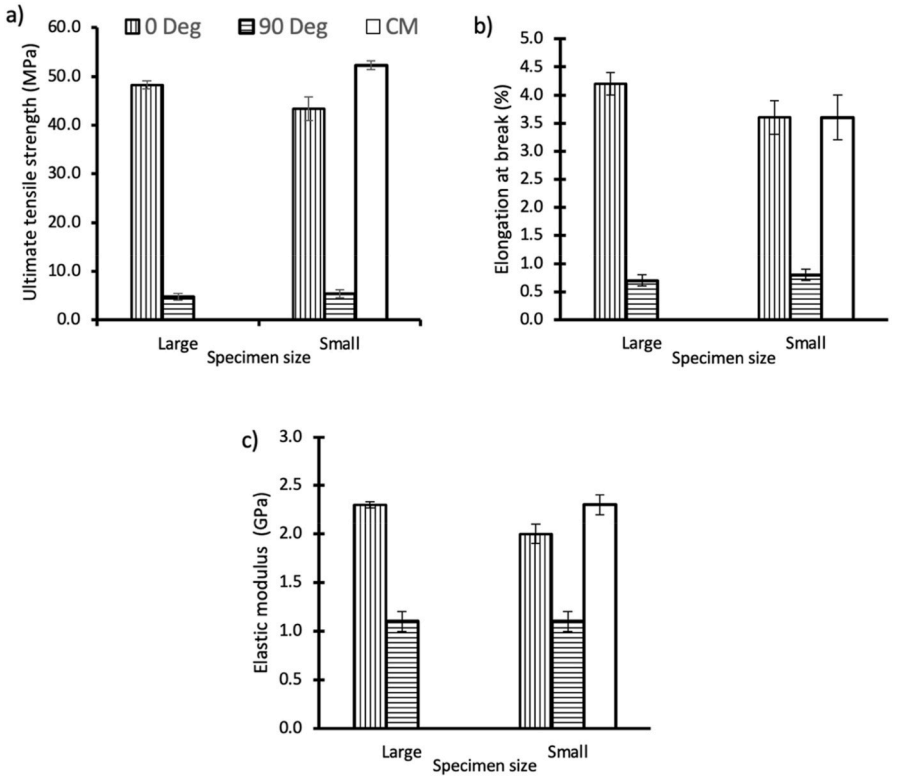

Fig. 16. Bar chart of the average tensile properties and standard deviations of each ASTM D3039 specimen taken from 5 samples: (a) ultimate tensile strength, UTS; (b) elongation at break, EAB; and (c) elastic modulus, EM. Abbreviations: 0 Deg = 0° raster angle (FFF) specimens; 90 Deg = 90° raster angle (FFF) specimens; CM = compression moulded.

ANOVA analysis. In the results reported in Table 5, p-values lower than 0.05 mean that there is a significant interaction between the effects of the specimen size and the raster angle on the tensile properties of the printed parts, with the greatest significance reported for UTS. However, the subsequent simple main effect analysis, whose results are listed in Table 6, actually demonstrates that only the tensile properties of the

Table 4
Tensile specimens tested in this case study.

Specimen label	Standard	Size (mm)	Manufacturing method, raster angle
Dogbone_0	ASTM D638 Type I	As per Fig. 9 (a)	FFF, 0°
Dogbone_90	ASTM D638 Type I	As per Fig. 9 (a)	FFF, 90°
Large_0	ASTM D3039	25 × 229 × 3	FFF, 0°
Small_0	ASTM D3039	22 × 220 × 3	FFF, 0°
Large_90	ASTM D3039	25 × 229 × 3	FFF, 90°
Small_90	ASTM D3039	22 × 220 × 3	FFF, 90°
Small_CM	ASTM D3039	22 × 220 × 3	Compression moulded

specimens printed at 0° are significantly affected by the specimen size, whereby larger components possess significantly higher values of UTS, EAB, and EM than the smaller counterparts. The variation in specimen size does not seem to significantly impact the UTS, EAB, and EM of the specimens printed at 90° raster angles, as they all have p-values exceeding 0.05.

Based on these tensile test results, it was confirmed that FFF parts exhibited significant anisotropic properties governed by the raster angle, and that the values obtained from tensile tests were affected by the size of the printed samples, even if the standard specification (in this case, according to ASTM D3039) were met. Between these two factors, the raster angle had more influence on the tensile properties, with an average contribution of 98.6% in the tensile test, as compared to a contribution of 35.2% coming from the size of the specimens.

As seen in Fig. 17, this may arise from the distinct failure modes imposed by the different raster angles. For 0° raster angle specimens, the occasional appearance of strained rasters and ultimately the specimen failure caused by the coordinated rupture of the individual rasters indicated that the rasters bore a significant portion of the applied tensile load. In spite of the necking incidentally observed within the individual rasters, the 0° raster angle specimens still experienced a brittle failure, without producing an overall plastic deformation, likely due to the weak inter-raster bonding. On the other hand, the smooth fractured surfaces of

Table 5
ANOVA analysis results.

	Dependent variable	Type III sum of squares	df	Mean square	F	p-value	Contribution (%)
Raster angle	**UTS**	8284.08	1	8284.08	4301.32	<.001	99.6
	EAB	50.562	1	50.562	1096.79	<.001	98.6
	EM	5.607	1	5.607	675.184	<.001	97.7
Specimen size	**UTS**	22.26	1	22.260	11.558	0.004	41.9
	EAB	0.288	1	0.288	6.247	0.024	28.1
	EM	0.073	1	0.073	8.815	0.009	35.5
Raster angle * specimen size	**UTS**	40.613	1	40.613	21.087	<.001	56.9
	EAB	0.648	1	0.648	14.056	0.002	46.8
	EM	0.049	1	0.049	5.901	0.027	26.9

Table 6
Simple main effect analysis results.

Dependent Variable	Raster angle (°)	(I) Size	(J) Size	Mean Difference (I-J)	Std. Error	p-value	95% Confidence Interval for Difference	
							Lower Bound	***Upper Bound***
UTS	0	Large	Small	4.960*	0.878	<.001	3.099	6.821
		Small	Large	−4.960*	0.878	<.001	−6.821	−3.099
	90	Large	Small	−0.74	0.878	0.412	−2.601	1.121
		Small	Large	0.74	0.878	0.412	−1.121	2.601
EAB	0	Large	Small	.600*	0.136	<.001	0.312	0.888
		Small	Large	−.600*	0.136	<.001	−0.888	−0.312
	90	Large	Small	−0.12	0.136	0.39	−0.408	0.168
		Small	Large	0.12	0.136	0.39	−0.168	0.408
EM	0	Large	Small	.220*	0.058	0.002	0.098	0.342
		Small	Large	−.220*	0.058	0.002	−0.342	−0.098
	90	Large	Small	0.022	0.058	0.708	−0.1	0.144
		Small	Large	−0.022	0.058	0.708	−0.144	0.1

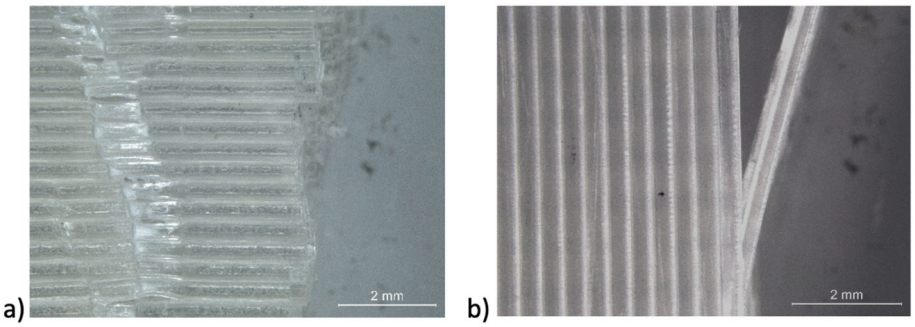

Fig. 17. Optical images of the ASTM D3039 tensile specimens after tensile testing: (a) 0° raster angle, and (b) 90° raster angle. The failure mode was the same for both Large and Small specimens. Scale bar: 2 mm.

the 90° specimens signified that the failure occurred due to raster-raster delamination, which suggests that the raster interfaces, rather than the rasters themselves, withstood most of the load. Generally, weak inter-raster and inter-layer bonding has been considered a major limitation to the mechanical properties of FFF parts [81]. Accordingly, since the raster interfaces possessed lower tensile stress bearing capacity than the highly dense rasters laid along the loading direction, the 0° specimens demonstrated higher tensile strength compared to the 90° specimens.

5.3.3. *Interaction effect of the specimen size and the raster angle*

As discussed, the effect of the specimen size was only substantial to specimens that were printed at 0° raster angle, and less important for the 90° orientation. In other terms, while the Large_0 specimens performed better than the Small_0 ones, the Large_90 specimens performed comparably to the Small_90 ones. At present, only two different sizes have been compared, and additional research is certainly needed to elaborate the effect of the specimen size on a wider range of dimensions. This would help confirm the strong effect of the specimen size on the 0° raster angle specimens, and to clarify the trend with respect to the 90° raster angle specimens. In fact, although the change in tensile properties for the 90° raster angle specimens was irrelevant according to the simple main effect analysis, it cannot be completely ruled out that increasing the difference in specimen size under this print orientation may ultimately lead to significant differences in the measured values of the tensile properties.

The X-ray analysis conducted on the tensile specimens (detail in Fig. 18) confirmed that the degree of crystallinity was around 0.52% after compression moulding and varied between around 0.33% and around 0.68% after 3D printing, with the height of the crystalline peak above the amorphous peak being comparable for all samples.

Since the degree of crystallinity is extremely low, and basically the same for all the specimens under exam, the complicated interplay between specimen size and print orientation, on the one hand, and measured tensile properties, on the other hand, should be rather attributed to the different thermal history and to geometric effects. Since the printing time is longer, larger parts reside at high temperature for a longer time. As long as the degree of crystallinity remains unaffected, the longer time at high temperature may help improve the interfaces between neighbouring rasters and layers through polymer-interdiffusion, and may also mitigate residual stresses [175]. The internal porosity associated with the interfacial bonding between the rasters and layers of the printed specimens obtained from μCT scans is shown in Fig. 19. The poor interfacial bonding between the rasters can be inferred from the presence of internal voids in all 3D printed samples, whereas voids are absent in the homogenous structure of compression moulded samples. However, it was clear that the longer thermal exposure enhanced the quality of interfacial bonding, as evident from the lower porosity observed in larger specimens as compared to the corresponding smaller counterparts. The substantial reduction in porosity may justify the statistically relevant improvement in tensile properties recorded upon increasing the size of the 0° raster angle specimens. Similar advantages should also be observed for the 90° raster angle specimens. However, for these specimens the reduction in porosity is less substantial, likely due to the different local temperature profiles associated with different toolpaths. Moreover, due to geometrical factors, whilst the defect density slightly decreases, the absolute number of raster interfaces unfavourably oriented in 90° raster angle specimens increases significantly when the size is increased, and this increases the likelihood of having at least one weak interface that will trigger the specimen's failure [201]. Since the orientation of the raster interfaces in 90° raster angle specimens is normal to the applied load, the increased probability of having a defective interface is particularly prejudicial to the tensile properties, and this is likely to counterbalance the positive effects coming from the longer thermal exposure. However, as already mentioned, these hypothetical explanations should be fact-checked against a wider range of specimen sizes.

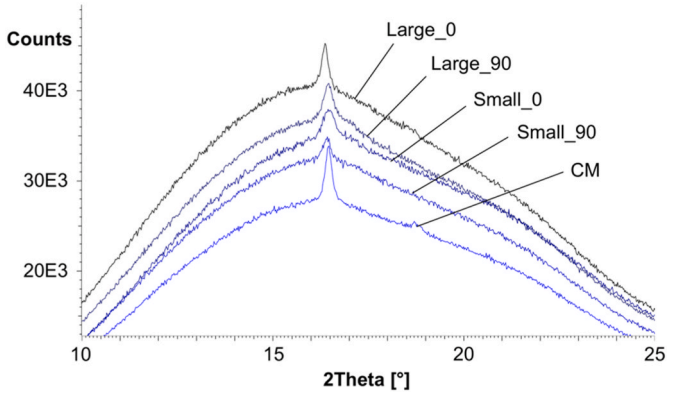

Fig. 18. XRD diffraction patterns of the specimens complying with ASTM D3030 (angular range: 10°–25° 2Theta). Abbreviations: CM = Compression moulded.

5.3.4. *Comparison between FFF parts and compression moulded parts*

Lastly, Small specimens printed according to ASTM D3039 were compared against compression moulded counterparts. Due to the absence of a raster- and layer-based structure, the compression moulded parts were assumingly more homogeneous than the FFF parts, and thus they were considered as a reference point for the tensile properties of the printed components. Among all the tensile properties, the UTS was affected the most by the fabrication technique, as the UTS of the small 0° and 90° raster angle specimens was 17% and 89.7% lower, respectively, when compared against the UTS of the compression moulded samples. The FFF parts, even with 0° rasters, were still found to be weaker than the compression moulded parts. As previously pointed out, the inter-raster voids, presented in Fig. 20, are likely to reduce the actual load-bearing cross-sectional area, and thus, the load bearing capacity of the printed parts.

6. Discussion

Mechanical testing is a crucial part of research in materials science, and also plays a key role in any manufacturing process. In particular, tensile testing is so popular that tensile properties are often identified as "the" mechanical properties as a whole. However, the lack of dedicated standards that outline how AM parts should be reliably and repeatably tested poses substantial challenges to the AM community. In the absence of specific guidelines, existing standards are currently being applied to AM specimens. However, current standards are unable to account for the complex hierarchical structure of AM parts. At present, numerous works have highlighted the urgent need to standardise processing parameters related to the meso-structure of AM parts, such as build orientation, infill degree, infill pattern, layer height, air gap, raster angle, raster width, etc. However, as clearly demonstrated in this review on FFF, this may be not enough, since the hierarchical structure of FFF parts subverts pre-existing concepts about the specimen geometry, undermines all size effect laws, and ultimately negates the applicability of conventional standards. This is further substantiated by the statistical analysis of the tensile properties of PLA parts measured according to ASTM D638 and ASTM D3039, which are clearly affected by the specimen geometry and size. The impact of the specimen geometry and size is still relatively underexplored in the literature, and yet it is critical, since the inconsistency of the acquired data impairs any sound comparison of the information published in the literature and even in technical reports. In reference to the existing standards, the specimen geometries for tensile testing of FFF parts are commonly in dumbbell and rectangular shapes. Despite that, the optimum choice between these two geometries remains controversial. The scrutiny of the literature conducted here, supported by the experimental findings, confirmed that rectangular coupons

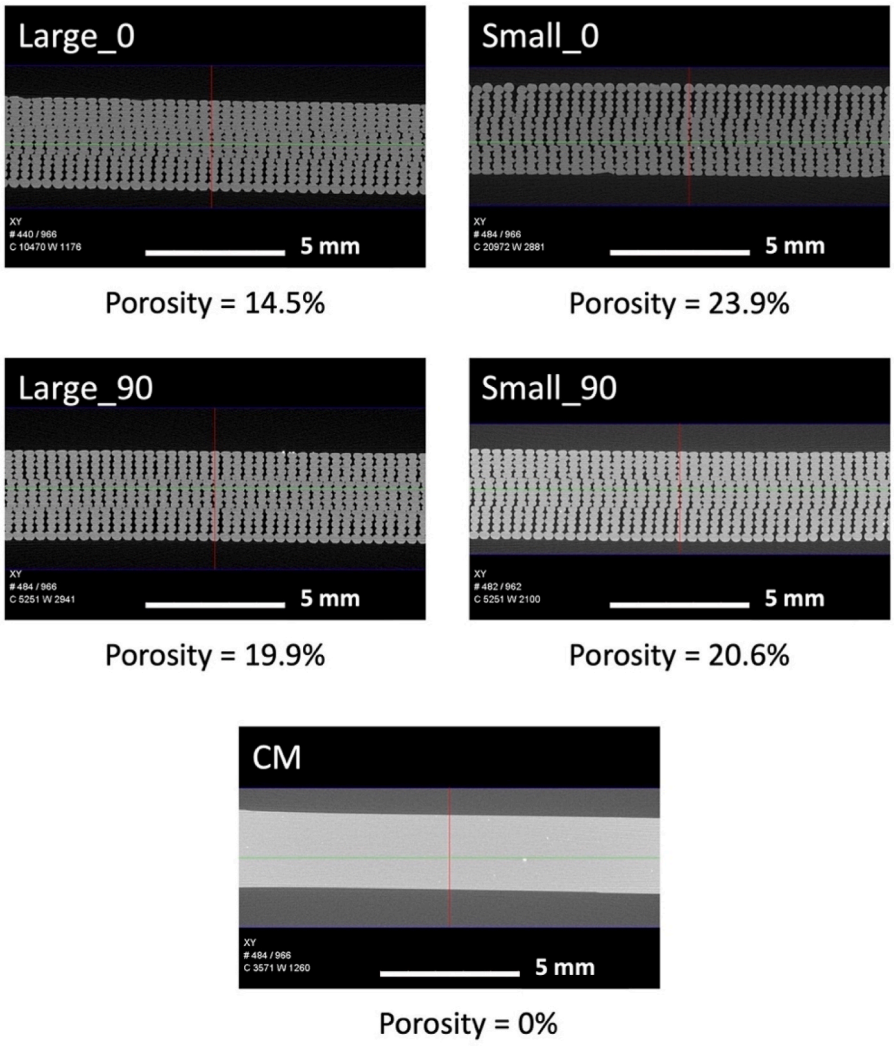

Fig. 19. μCT scans of FFF specimens showing the raster's cross section. The compression moulded (CM) specimen is also included as a term of comparison.

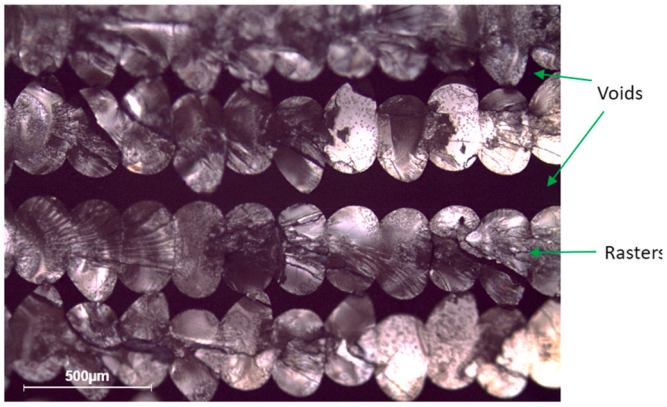

Fig. 20. Optical image of the inter-raster voids that were present in 0° raster angle specimens. Scale bar: 500 μm.

should be preferred to the dumbbell-like geometries, as the straight edges eliminate abrupt transition zones, and minimise premature failure induced by stress concentration. Whilst contradictory trends have been reported in the literature, the statistical analysis of the tensile properties of the PLA specimens as per ASTM D3039 in the present contribution suggests that the size of the specimens affects the measured tensile properties depending on the mesostructure of the specimens, since the effect of the specimen size was only evident in coupons printed at 0° raster angle. In other terms, for FFF parts size-related effects appear to be an anisotropic phenomenon. Owing to the hierarchical structure of FFF parts, it may be hypothesised that this interplay between the size effect and the print orientation (raster angle) actually originates from microstructural details, such as inter-raster pores, weak raster-raster interfaces, and intra-raster defects that may vary according to the processing parameters. This corroborates the idea that FFF parts are architectured materials, whose macroscale behaviour stems from structural features across multiple length scales.

Ultimately, this poses the question of whether regulating the aforementioned processing parameters, specimen geometry, and size will be sufficient to account for the multiscale effects and finally lead to the definition of appropriate FFF test protocols.

7. Conclusions

The development of dedicated international standards is a compelling need to enable the wider uptake of additive manufacturing (AM) in industry, to benchmark new materials and products against conventionally fabricated ones, and to set the basis for a sound understanding and comparison among the functional and mechanical properties of 3D printed parts as published in scientific papers and in technical data sheets. Several standards developing organisations (SDOs) worldwide

are now working to satisfy this demand and stimulate the advancement of knowledge, research, and technology through the development of standards for AM. However, the current lack of specific standards that outline how to measure and report the tensile properties of AM parts still requires immediate attention. On the one hand, tensile properties are so popular that they are often identified as the "mechanical properties", tout court. On the other hand, existing standards for the determination of the tensile properties of conventional materials are not immediately applicable to AM parts. For the first time, this review gathers rich information from the available literature to clearly demonstrate these hurdles with parts produced by fused filament fabrication (FFF), which is currently the most widespread polymer-based AM method. The analysis of the literature indicates that existing standards are unable to account for the numerous parameters involved in FFF, although they influence the mechanical behaviour. Until dedicated standards become available for FFF, the exact processing parameters and condition should be fully reported alongside the testing parameters in order to ensure the repeatability of the test. Moreover, the raster- and layer-based build-up of 3D parts and the complicated interplay of structural features across different length scales in FFF undermine the reliability of results obtained from dumbbell-like specimens and erode all classical theories regarding the size effect. The complicated trends emerging from the body of literature are here confirmed by a case study, whereby the statistical analysis of the tensile properties of poly(lactic acid) (PLA) parts measured according to ASTM D638 (type I) and ASTM D3039 proves that the experimental results are affected by the specimen geometry and size. Although future research should certainly be addressed to capturing the scale-related effects on a larger set of specimen sizes, the available data suggest that (i) rectangular coupons with straight edges like ASTM D3039 should be preferred to dumbbell-like ones with curved edges like ASTM D638 in order to achieve a higher compliance to the failure criterion, and that (ii) the specimen size influences the tensile behaviour, often with contrasting results. The opposing trends reported in the literature may be attributed to numerous variables, such as the kind of feedstock in use (amorphous vs. semi-crystalline, neat polymer vs. composite material, etc), the printer set-up and printing parameters, and even the testing conditions applied. The experimental campaign conducted here on the PLA specimens proved that anisotropic effects may also contribute to this uncertainty, since only the tensile properties of the specimens printed at 0° raster angle were significantly affected by the specimen size, with the larger specimens achieving significantly higher values of the Young's modulus (stiffness), ultimate tensile stress (strength), and elongation at break (toughness). Conversely, the variation in specimen size did not seem to significantly impact the tensile properties of the specimens printed at 90° raster angle. As such, whilst the adoption of simple rectangular coupons having a fixed (standardised) size may be a convenient avenue of obtaining repeatable tensile properties for polymer parts produced by FFF, it is still questionable whether these results would be representative of the behaviour of different, and often more complicated, 3D printed constructs. This may become critical on account of the increasing popularity of polymer AM for producing load bearing structures, lightweight components and topologically optimised constructs, whose design is far from being comparable to a base rectangle.

Author statement

Antonella Sola: Conceptualisation, Methodology, Investigation, Writing – Original draft, Writing – Review & Editing, Supervision, Project administration, Funding acquisition, Wei Juene Chong: Formal analysis, Data curation, Investigation, Writing – Original draft, Writing – Review & Editing, Dejana Pejak Simunec: Formal analysis, Data curation, Investigation, Writing – Review & Editing, Yuncang Li: Project management; Writing – Review & Editing, Adrian Trinchi: Project management; Writing – Review & Editing, Ilias (Louis) Kyratzis: Project management; Writing – Review & Editing, Cuie Wen: Conceptualisation, Writing – Original draft, Writing – Review & Editing, Supervision, Project administration, Funding acquisition.

Declaration of competing interest

The authors declare that they have no known competing financial interests or personal relationships that could have appeared to influence the work reported in this paper.

Data availability

Data will be made available on request.

Acknowledgments

CW and YL are supported by the Australian Research Council (ARC) through the discovery grant DP210101862.

AS and DPS are supported by the Commonwealth Scientific and Industrial Research Organisation (CSIRO) Research Office through the "Science Leader in Active Materials" grant.

References

[1] ISO/ASTM 52900, ISO/ASTM 52900:2021, Additive Manufacturing — General Principles — Fundamentals and Vocabulary, Technical Committee ISO/TC 261 Additive Manufacturing, 2021.

[2] A. Cano-Vicent, M.M. Tambuwala, S.S. Hassan, D. Barh, A.A. Aljabali, M. Birkett, A. Arjunan, Á. Serrano-Aroca, Fused deposition modelling: current status, methodology, applications and future prospects, Addit. Manuf. 47 (2021), 102378, https://doi.org/10.1016/j.addma.2021.102378.

[3] S.M.F. Kabir, K. Mathur, A.-F.M. Seyam, A critical review on 3D printed continuous fiber-reinforced composites: history, mechanism, materials and properties, Compos. Struct. 232 (2020), 111476, https://doi.org/10.1016/j.compstruct.2019.111476.

[4] C.K. Chua, C.H. Wong, W.Y. Yeong, 2 – roadmap on additive manufacturing standards, in: Standards, Quality Control, and Measurement Sciences in 3D Printing and Additive Manufacturing, Academic Press, Elsevier, London, UK – San Diego, CA, United States – Cambridge, MA, United States – Kidlington, Oxford, UK, 2017, pp. 31–55, https://doi.org/10.1016/B978-0-12-813489-4.00002-7.

[5] S.A.M. Tofail, E.P. Koumoulos, A. Bandyopadhyay, S. Bose, L. O'Donoghue, C. Charitidis, Additive manufacturing: scientific and technological challenges, market uptake and opportunities, Mater. Today 21 (2018) 22–37, https://doi.org/10.1016/j.mattod.2017.07.001.

[6] Z. Chen, C. Han, M. Gao, S.Y. Kandukuri, K. Zhou, A review on qualification and certification for metal additive manufacturing, Virtual Phys. Prototyp. 17 (2022) 382–405, https://doi.org/10.1080/17452759.2021.2018938.

[7] L. Crocker, Literature Review on Tensile Test Standards for Metal Additive Manufacturing. NPL Report MAT 89, NPL Management Limited, National Physical Laboratory, Middlesex, UK, 2019. ISSN 1754-2979 Available on-line at: https://eprintspublications.npl.co.uk/8508/1/MAT89.pdf. (Accessed 26 June 2022).

[8] N. Hrabe, N. Barbosa, S. Daniewicz, N. Shamsaei, Findings from the NIST/ASTM Workshop on Mechanical Behavior of Additive Manufacturing Components. NIST Advanced Manufacturing Series 100-4, National Institute of Standards and Technology, 2016, https://doi.org/10.6028/NIST.AMS.100-4, 10.6028/NIST.AMS.100-4. Available on-line at:. (Accessed 24 May 2022).

[9] L. Koester, H. Taheri, L.J. Bond, D. Barnard, J. Gray, Additive manufacturing metrology: state of the art and needs assessment, AIP Conf. Proc. 1706 (2016), 130001, https://doi.org/10.1063/1.4940604.

[10] L.S. Moura, G.D. Vittoria, A.H.G. Gabriel, E.B. Fonseca, L.P. Gabriel, T.J. Webster, E.S.N. Lopes, A highly accurate methodology for the prediction and correlation of mechanical properties based on the slimness ratio of additively manufactured tensile test specimens, J. Mater. Sci. 55 (2020) 9578–9596, https://doi.org/10.1007/s10853-020-04654-y.

[11] S. Moylan, J. Slotwinski, A. Cooke, K. Jurrens, A. Donmez, An additive manufacturing test artifact, J. Res. Natl. Inst. Stand. Technol. 119 (2014) 429–459, https://doi.org/10.6028/jres.119.017.

[12] R.A. Roach, S.H. Gardner, Cluster 1: commercializing additive manufacturing—hurdles in materials characterization and testing, Transl. Mater. Res. 4 (2017), 044001, https://doi.org/10.1088/2053-1613/aa8513.

[13] R. Russell, D. Wells, J. Waller, B. Poorganji, E. Ott, T. Nakagawa, H. Sandoval, N. Shamsaei, M. Seifi, 3 – qualification and certification of metal additive manufactured hardware for aerospace applications, in: F. Froes, R. Boyer (Eds.), Additive Manufacturing for the Aerospace Industry, Elsevier, Amsterdam, The Netherlands – Kidlington, Oxford UK – Cambridge, MA, United States, 2019, pp. 33–66, https://doi.org/10.1016/B978-0-12-814062-8.00003-0.

[14] M. Seifi, A. Salem, J. Beuth, O. Harrysson, J.J. Lewandowski, Overview of materials qualification needs for metal additive manufacturing, JOM 68 (2016) 747–764, https://doi.org/10.1007/s11837-015-1810-0.

[15] M. Seifi, M. Gorelik, J. Waller, N. Hrabe, N. Shamsaei, S. Daniewicz, J. J. Lewandowski, Progress towards metal additive manufacturing standardization to support qualification and certification, JOM 69 (2017) 439–455, https://doi.org/10.1007/s11837-017-2265-2.

[16] J.A. Slotwinski, S.P. Moylan, Applicability of Existing Materials Testing Standards for Additive Manufacturing Materials. NISTIR 8005, NIST, Gaithersburg, MD, 2014, https://doi.org/10.6028/NIST.IR.8005. Available on-line at:. (Accessed 24 May 2022).

[17] J.A. Slotwinski, E.J. Garboczi, Metrology needs for metal additive manufacturing powders, JOM 67 (2015) 538–543, https://doi.org/10.1007/s11837-014-1290-7.

[18] W.H. Ferrell, J. Clement, S. TerMaath, Uniaxial tensile testing standardization for the qualification of fiber reinforced plastics for fused filament fabrication, Mech. Adv. Mater. Struct. 28 (2021) 1254–1273, https://doi.org/10.1080/15376494.2019.1660438.

[19] M.R. Khosravani, F. Berto, M.R. Ayatollahi, T. Reinicke, Characterization of 3D-printed PLA parts with different raster orientations and printing speeds, Sci. Rep. 12 (2022) 1016, https://doi.org/10.1038/s41598-022-05005-4.

[20] S.J. Hollister, C.L. Flanagan, D.A. Zopf, R.J. Morrison, H. Nasser, J.J. Patel, E. Ebramzadeh, S.N. Sangiorgio, M.B. Wheeler, G.E. Green, Design control for clinical translation of 3D printed modular scaffolds, Ann. Biomed. Eng. 43 (2015) 774–786, https://doi.org/10.1007/s10439-015-1270-2.

[21] H.L. Tekinalp, V. Kunc, G.M. Velez-Garcia, C.E. Duty, L.J. Love, A.K. Naskar, C. A. Blue, S. Ozcan, Highly oriented carbon fiber–polymer composites via additive manufacturing, Compos. Sci. Technol. 105 (2014) 144–150, https://doi.org/10.1016/j.compscitech.2014.10.009.

[22] H.D. Vora, S. Sanyal, A comprehensive review: metrology in additive manufacturing and 3D printing technology, Prog. Addit. Manuf. 5 (2020) 319–353, https://doi.org/10.1007/s40964-020-00142-6.

[23] G.D. Goh, W. Toh, Y.L. Yap, T.Y. Ng, W.Y. Yeong, Additively manufactured continuous carbon fiber-reinforced thermoplastic for topology optimized unmanned aerial vehicle structures, Compos. B Eng. 216 (2021), 108840, https://doi.org/10.1016/j.compositesb.2021.108840.

[24] W. Wu, Q. Wang, W. Li, Comparison of tensile and compressive properties of carbon/glass interlayer and intralayer hybrid composites, Materials 11 (2018) 1105, https://doi.org/10.3390/ma11071105.

[25] A. Kehinde Aworinde, S. Oluropo Adeosun, F. Adekunle Oyawale, E. Titilayo Akinlabi, S.A. Akinlabi, Parametric effects of fused deposition modelling on the mechanical properties of polylactide composites: a review, J. Phys. Conf. Ser. 1378 (2019), 022060, https://doi.org/10.1088/1742-6596/1378/2/022060.

[26] S.-H. Ahn, M. Montero, D. Odell, S. Roundy, P.K. Wright, Anisotropic material properties of fused deposition modeling ABS, Rapid Prototyp. J. 8 (2002) 248–257, https://doi.org/10.1108/13552540210441166.

[27] M.D. Monzón, Z. Ortega, A. Martínez, F. Ortega, Standardization in additive manufacturing: activities carried out by international organizations and projects, Int. J. Adv. Manuf. Technol. 76 (2015) 1111–1121, https://doi.org/10.1007/s00170-014-6334-1.

[28] Sculpteo, The State of 3D Printing, 2021 Edition, 2021. Available on-line at: https://www.sculpteo.com/en/ebooks/state-of-3d- printing-report-2021/. (Accessed 1 September 2021).

[29] A.M. Forster, Materials Testing Standards for Additive Manufacturing of Polymer Materials: State of the Art and Standards Applicability, NISTIR 8059, NIST, Gaithersburg, MD, 2015, https://doi.org/10.6028/NIST.IR.8059.

[30] C. Phillips, M. Kortschot, F. Azhari, Towards standardizing the preparation of test specimens made with material extrusion: review of current techniques for tensile testing, Addit. Manuf. 58 (2022), 103050, https://doi.org/10.1016/j.addma.2022.103050.

[31] J. Gumpinger, M. Seifi, N. Shamsaei, C. Seidel, R.W. Russell, 20 - recent progress on global standardization, in: I. Yadroitsev, I. Yadroitsava, A. du Plessis, E. MacDonald (Eds.), Fundamentals of Laser Powder Bed Fusion of Metals, a Volume in Additive Manufacturing Materials and Technologies, Elsevier, Amsterdam, Netherlands – Kidlington, Oxford UK – Cambridge, MA, United States, 2021, pp. 563–582, https://doi.org/10.1016/B978-0-12-824090-8.00021-4.

[32] C.-J. Bae, A.B. Diggs, A. Ramachandran, 6 – quantification and certification of additive manufacturing materials and processes, in: J. Zhang, Y.-G. Jung (Eds.), Additive Manufacturing - Materials, Processes, Quantifications and Applications, Butterworth-Heinemann, Elsevier, Kidlington, Oxford, UK – Cambridge, MA, United States, 2018, pp. 181–213, https://doi.org/10.1016/B978-0-12-812155-9.00006-2.

[33] R. Udroiu, I.C. Braga, A. Nedelcu, Evaluating the quality surface performance of additive manufacturing systems: methodology and a material jetting case study, Materials 12 (2019) 995, https://doi.org/10.3390/ma12060995.

[34] ISO/ASTM 52902, ISO/ASTM 52902:2019, Additive Manufacturing – Test Artifacts – Geometric Capability Assessment of Additive Manufacturing Systems, Technical Committee ISO/TC 261 Additive Manufacturing, 2019.

[35] M.-A. de Pastre, S.-C. Toguem Tagne, N. Anwer, Test artefacts for additive manufacturing: a design methodology review, CIRP J. Manuf. Sci. Technol. 31 (2020) 14–24, https://doi.org/10.1016/j.cirpj.2020.09.008.

[36] A. Martínez-García, M. Monzón, R. Paz, 12 - standards for additive manufacturing technologies: structure and impact, in: J. Pou, A. Riveiro, J.P. Davim (Eds.), Additive Manufacturing. Handbooks in Advanced Manufacturing, Elsevier, Amsterdam, The Netherlands – Kidlington, Oxford, UK – Cambridge, MA, United States, 2021, pp. 395–408, https://doi.org/10.1016/B978-0-12-818411-0.00013-6.

[37] J. Bonnin Roca, E.R. Fuchs, P. Vaishnav, M.G. Morgan, J. Mendonça, When risks cannot be seen: regulating uncertainty in emerging technologies, Res. Pol. 46 (2017) 1215–1233, https://doi.org/10.1016/j.respol.2017.05.010.

[38] M. Aburaia, C. Bucher, M. Lackner, J. Gonzalez-Gutierrez, H. Zhang, H. Lammer, A production method for standardized continuous fiber reinforced FFF filament, Biomater. Med. Appl. 4 (2020), 1000123, https://doi.org/10.37532/bma.2020.4(1).123.

[39] C.K. Chua, C.H. Wong, W.Y. Yeong, 3 – measurement science roadmap for additive manufacturing, in: Standards, Quality Control, and Measurement Sciences in 3D Printing and Additive Manufacturing, Academic Press, Elsevier, London, UK – San Diego, CA, United States – Cambridge, MA, United States – Kidlington, Oxford, UK, 2017, pp. 57–73, https://doi.org/10.1016/B978-0-12-813489-4.00003-9.

[40] L.R. Meza, J.R. Greer, Mechanical characterization of hollow ceramic nanolattices, J. Mater. Sci. 49 (2014) 2496–2508, https://doi.org/10.1007/s10853-013-7945-x.

[41] A. Dal Maso, F. Cosmi, Mechanical characterization of 3D-printed objects, Mater. Today Proc. 5 (2018) 26739–26746, https://doi.org/10.1016/j.matpr.2018.08.145.

[42] C. Badini, E. Padovano, R. De Camillis, V.G. Lambertini, M. Pietroluongo, Preferred orientation of chopped fibers in polymer-based composites processed by selective laser sintering and fused deposition modeling: effects on mechanical properties, J. Appl. Polym. Sci. 137 (2020), e49152, https://doi.org/10.1002/app.49152.

[43] B.M. Tymrak, M. Kreiger, J.M. Pearce, Mechanical properties of components fabricated with open-source 3-D printers under realistic environmental conditions, Mater. Des. 58 (2014) 242–246, https://doi.org/10.1016/j.matdes.2014.02.038.

[44] T.J. Gordelier, P.R. Thies, L. Turner, L. Johanning, Optimising the FDM additive manufacturing process to achieve maximum tensile strength: a state-of-the-art review, Rapid Prototyp. J. 25 (2019) 953–971, https://doi.org/10.1108/RPJ-07-2018-0183.

[45] E.H. Baran, H.Y. Erbil, Surface modification of 3D printed PLA objects by fused deposition modeling: a review, Colloids and Interfaces 3 (2019) 43, https://doi.org/10.3390/colloids3020043.

[46] J.S. Chohan, R. Singh, Pre and post processing techniques to improve surface characteristics of FDM parts: a state of art review and future applications, Rapid Prototyp. J. 23 (2017) 495–513, https://doi.org/10.1108/RPJ-05-2015-0059.

[47] R. Kawalkar, H.K. Dubey, S.P. Lokhande, A review for advancements in standardization for additive manufacturing, Mater, Today Off.: SAVE Proc. 50 (2022) 1983–1990, https://doi.org/10.1016/j.matpr.2021.09.333.

[48] A.R. Torrado, D.A. Roberson, Failure analysis and anisotropy evaluation of 3D-printed tensile test specimens of different geometries and print raster patterns, J. Fail. Anal. Prev. 16 (2016) 154–164, https://doi.org/10.1007/s11668-016-0067-4.

[49] R.A. Roach, J.E. Bishop, K. Johnson, T. Rodgers, B.L. Boyce, L. Swiler, B. van Bloemen Waanders, M. Chandross, D. Kammler, D. Balch, B. Jared, M.J. Martinez, N. Leathe, K. Ford, Using additive manufacturing as a pathway to change the qualification paradigm, in: Solid Freeform Fabrication 2018: Proceedings of the 29th Annual International Solid Freeform Fabrication Symposium – an Additive Manufacturing Conference, vol. 1, The University of Texas at Austin, Austin, Texas, USA, 2018, pp. 3–13, https://doi.org/10.26153/tsw/16995. August 13-15.

[50] X. Zhou, S.-J. Hsieh, C.-C. Ting, Modelling and estimation of tensile behaviour of polylactic acid parts manufactured by fused deposition modelling using finite element analysis and knowledge-based library, Virtual Phys. Prototyp. 13 (2018) 177–190, https://doi.org/10.1080/17452759.2018.1442681.

[51] D. Eisenbarth, P. Stoll, C. Klahn, T.B. Heinis, M. Meboldt, K. Wegener, Unique coding for authentication and anti-counterfeiting by controlled and random process variation in L-PBF and L-DED, Addit. Manuf. 35 (2020), 101298, 1164 10.1016/j.addma.2020.101298.

[52] D. Popescu, A. Zapciu, C. Amza, F. Baciu, R. Marinescu, FDM process parameters influence over the mechanical properties of polymer specimens: a review, Polym. Test. 69 (2018) 157–166, https://doi.org/10.1016/j.polymertesting.2018.05.020.

[53] R. Shrestha, N. Shamsaei, M. Seifi, N. Phan, An investigation into specimen property to part performance relationships for laser beam powder bed fusion additive manufacturing, Addit. Manuf. 29 (2019), 100807, https://doi.org/10.1016/j.addma.2019.100807.

[54] ASTM F2971, ASTM F2971-13(2021). Standard Practice for Reporting Data for Test Specimens Prepared by Additive Manufacturing. Book of Standards Volume: 10.04, Developed by Subcommittee: F42.01, 2021, https://doi.org/10.1520/F2971-13R21.

[55] ISO/ASTM 52921, ISO/ASTM 52921:2013, Standard Terminology for Additive Manufacturing — Coordinate Systems and Test Methodologies, Technical Committee ISO/TC 261 Additive Manufacturing, 2013.

[56] J.J. Laureto, J.M. Pearce, Anisotropic mechanical property variance between ASTM D638-14 type I and type IV fused filament fabricated specimens, Polym. Test. 68 (2018) 294–301, https://doi.org/10.1016/j.polymertesting.2018.04.029.

[57] K. Carpenter, A. Tabei, On residual stress development, prevention, and compensation in metal additive manufacturing, Materials 13 (2020) 255, https://doi.org/10.3390/ma13020255.

[58] A.A. Samy, A. Golbang, E. Harkin-Jones, E. Archer, M. Dahale, A. McIlhagger, Influence of ambient temperature on part distortion: a simulation study on

amorphous and semi-crystalline polymer, Polymers 14 (2022) 879, https://doi.org/10.3390/polym14050879.
[59] AM CoE, ASTM Additive Manufacturing Center of Excellence, Strategic Roadmap for Research and Development, Public Version, April 2020, 2020. Available on-line through: https://amcoe.org/s/AM-CoE-Roadmap-R8.pdf. (Accessed 14 June 2022).
[60] NIST, Measurement Science Roadmap for Metal-Based Additive Manufacturing. Workshop Summary Report, May 2013. Available on-line at: https://www.nist.gov/system/files/documents/el/isd/NISTAdd_Mfg_Report_FINAL-2.pdf. (Accessed 26 June 2022).
[61] K. Migler, R. Ricker, Measurement Science Roadmap for Polymer-Based Additive Manufacturing. Advanced Manufacturing Series (NIST AMS), National Institute of Standards and Technology, Gaithersburg, MD, 2016, https://doi.org/10.6028/NIST.AMS.100-5, 10.6028/NIST.AMS.100-5. Available on-line at:. (Accessed 26 June 2022).
[62] AMSC (Additive Manufacturing Standardization Collaborative), Standardization Roadmap for Additive Manufacturing, in: Version 2.0, ANSI and NDCMM/America Makes, 2018, 2018. Available on-line through: https://www.ansi.org/standards-coordination/collaboratives-activities/additive-manufacturing-collaborative (registration required).
[63] ASTM Standardization news, ASTM and ISO Sign Additive Manufacturing PSDO Agreement. Standardization News 2011, 2011. Issue month November/December. Available on-line: https://sn.astm.org/?q=outreach/astm-and-iso-sign-additive-manufacturing-psdo-agreement-nd11.html. (Accessed 9 June 2022).
[64] C. Naden, ISO and ASTM International Unveil Framework for Creating Global Additive Manufacturing Standards, International Organization for Standardization. ISO News, 2016 published 7 October, https://www.iso.org/news/2016/10/Ref2124.html. (Accessed 9 June 2022). Available on-line:.
[65] G. Moroni, S. Petrò, H. Shao, On standardization efforts for additive manufacturing, in: L. Wang, V. Majstorovic, D. Mourtzis, E. Carpanzano, G. Moroni, L. Galantucci (Eds.), Proceedings of 5th International Conference on the Industry 4.0 Model for Advanced Manufacturing. Lecture Notes in Mechanical Engineering, Springer, Cham, Switzerland, 2020, pp. 156–172, https://doi.org/10.1007/978-3-030-46212-3_11.
[66] ASTM ISO/ASTM 52907, ICS Code: 25.030, ASTM ISO/ASTM 52907:2019. Additive Manufacturing — Feedstock Materials — Methods to Characterize Metal Powders, Book of Standards, 10.04, 2019, https://doi.org/10.1520/F3382-19. Developed by Subcommittee: F42.01.
[67] ASTM F3571, ASTM F3571-22: Standard Guide for Sdditive Manufacturing – Feedstock – Particle Shape Image Analysis by Optical Photography to Identify and Quantify the Agglomerates/satellites in Metal Powder Feedstock. Book of Standards, 10.04, 2022, https://doi.org/10.1520/F3571-22. Developed by Subcommittee: F42.01.
[68] ASTM F3122, ASTM F3122-14(2022). Standard Guide for Evaluating Mechanical Properties of Metal Materials Made via Additive Manufacturing Processes. Book of Standards, 10.04, 2022, https://doi.org/10.1520/F3122-14R22. Developed by Subcommittee: F42.01.
[69] ISO 27547-1, ISO 27547-1:2010, Plastics — Preparation of Test Specimens of Thermoplastic Materials Using Mouldless Technologies — Part 1: General Principles, and Laser Sintering of Test Specimens, Technical Committee: ISO/TC 261 Additive manufacturing, 2010.
[70] ISO/ASTM TR 52906, ISO/ASTM TR 52906:2022, Additive Manufacturing — Non-destructive Testing — Intentionally Seeding Flaws in Metallic Parts, Technical Committee ISO/TC 261 Additive manufacturing, 2022.
[71] ISO 17296-3, ISO 17296-3:2014, Additive Manufacturing — General Principles — Part 3: Main Characteristics and Corresponding Test Methods, Technical Committee: ISO/TC 261 Additive manufacturing, 2014.
[72] C.K. Chua, C.H. Wong, W.Y. Yeong, 4 – software and data format, in: Standards, Quality Control, and Measurement Sciences in 3D Printing and Additive Manufacturing, Academic Press, Elsevier, London, UK – San Diego, CA, United States – Cambridge, MA, United States – Kidlington, Oxford, UK, 2017, pp. 75–94, https://doi.org/10.1016/B978-0-12-813489-4.00004-0.
[73] ISO/ASTM 52915, ISO/ASTM 52915:2020, Specification for Additive Manufacturing File Format (AMF) Version 1.2, Technical Committee ISO/TC 261 Additive manufacturing, 2020.
[74] T.J. Coogan, D.O. Kazmer, Bond and part strength in fused deposition modeling, Rapid Prototyp. J. 23 (2017) 414–422, https://doi.org/10.1108/RPJ-03-2016-0050.
[75] B.N. Turner, R. Strong, S.A. Gold, A review of melt extrusion additive manufacturing processes: I. Process design and modeling, Rapid Prototyp. J. 20 (2014) 192–204, https://doi.org/10.1108/RPJ-01-2013-0012.
[76] Y. Kok, X.P. Tan, P. Wang, M.L.S. Nai, N.H. Loh, E. Liu, S.B. Tor, Anisotropy and heterogeneity of microstructure and mechanical properties in metal additive manufacturing: a critical review, Mater. Des. 139 (2018) 565–586, https://doi.org/10.1016/j.matdes.2017.11.021.
[77] N. Zohdi, R. Yang, Material anisotropy in additively manufactured polymers and polymer composites: a review, Polymers 13 (2021) 3368, https://doi.org/10.3390/polym13193368.
[78] T. Yao, Z. Deng, K. Zhang, S. Li, A method to predict the ultimate tensile strength of 3D printing polylactic acid (PLA) materials with different printing orientations, Compos. B Eng. 163 (2019) 393–402, https://doi.org/10.1016/j.compositesb.2019.01.025.
[79] C.-Y. Liaw, J.W. Tolbert, L.W. Chow, M. Guvendiren, Interlayer bonding strength of 3D printed PEEK specimens, Soft Matter 17 (2021) 4775–4789, https://doi.org/10.1039/d1sm00417d.
[80] J. Spadaro, Cartesian vs. delta printers: how do they work?, 3D printing, articles/How it works. No data. Available on-line at: https://www.printspace3d.com/cartesian-vs-delta-printers-work/. (Accessed 26 June 2022).
[81] X. Gao, S. Qi, X. Kuang, Y. Su, J. Li, D. Wang, Fused filament fabrication of polymer materials: a review of interlayer bond, Addit. Manuf. 37 (2021), 101658, https://doi.org/10.1016/j.addma.2020.101658.
[82] A.E. Costa, A.F. da Silva, O.S. Carneiro, A study on extruded filament bonding in fused filament fabrication, Rapid Prototyp. J. 25 (2018) 555–565, https://doi.org/10.1108/RPJ-03-2018-0062.
[83] M.E. Mackay, The importance of rheological behavior in the additive manufacturing technique material extrusion, J. Rheol. 62 (2018) 1549–1561, https://doi.org/10.1122/1.5037687.
[84] A. Sola, Materials requirements in fused filament fabrication: a framework for the design of next-generation 3D printable thermoplastics and composites, Macromol. Mater. Eng. 307 (10) (2022), 2200197, https://doi.org/10.1002/mame.202200197.
[85] Q. Sun, G.M. Rizvi, C.T. Bellehumeur, P. Gu, Effect of processing conditions on the bonding quality of FDM polymer filaments, Rapid Prototyp. J. 14 (2008) 72–80, https://doi.org/10.1108/13552540810862028.
[86] F. Yang, R. Pitchumani, Healing of thermoplastic polymers at an interface under nonisothermal conditions, Macromolecules 35 (2002) 3213–3224, https://doi.org/10.1021/ma010858o.
[87] J.E. Seppala, K.D. Migler, Infrared thermography of welding zones produced by polymer extrusion additive manufacturing, Addit. Manuf. 12 (2016) 71–76, https://doi.org/10.1016/j.addma.2016.06.007.
[88] K. Balani, V. Verma, A. Agarwal, R. Narayan, A, 1 – physical, thermal, and mechanical properties of polymers, in: K. Balani, V. Verma, A. Agarwal, R. Narayan (Eds.), Biosurfaces: A Materials Science and Engineering Perspective, John Wiley & Sons, Inc., Hoboken, NJ, USA, 2014, pp. 329–344, https://doi.org/10.1002/9781118950623.app1.
[89] D. Vaes, M. Coppens, B. Goderis, W. Zoetelief, P. Van Puyvelde, The extent of interlayer bond strength during fused filament fabrication of nylon copolymers: an interplay between thermal history and crystalline morphology, Polymers 13 (2021) 2677, https://doi.org/10.3390/polym13162677.
[90] Y. Tao, F. Kong, Z. Li, J. Zhang, X. Zhao, Q. Yin, D. Xing, P. Li, A review on voids of 3D printed parts by fused filament fabrication, J. Mater. Res. Technol. 15 (2021) 4860–4879, https://doi.org/10.1016/j.jmrt.2021.10.108.
[91] A. Elkholy, M. Roubi, R. Kempers, Characterization of the anisotropic thermal conductivity of additively manufactured components by fused filament fabrication, Prog. Addit. Manuf. 4 (2019) 497–515, https://doi.org/10.1007/s40964-019-00098-2.
[92] D. Pejak Simunec, A. Sola, Emerging research in conductive materials for fused filament fabrication: a critical review, Adv. Eng. Mater. 2022 (2022), 2101476, https://doi.org/10.1002/adem.202101476.
[93] B. Huang, S. Singamneni, Raster angle mechanics in fused deposition modelling, J. Compos. Mater. 49 (2015) 363–383, https://doi.org/10.1177/0021998313519153.
[94] C. Casavola, A. Cazzato, V. Moramarco, C. Pappalettere, Orthotropic mechanical properties of fused deposition modelling parts described by classical laminate theory, Mater. Des. 90 (2016) 453–458, https://doi.org/10.1016/j.matdes.2015.11.009.
[95] L. Li, Q. Sun, C. Bellehumeur, P. Gu, Composite modeling and analysis for fabrication of FDM prototypes with locally controlled properties, J. Manuf. Process. 4 (2002) 129–141, https://doi.org/10.1016/S1526-6125(02)70139-4.
[96] M. Somireddy, A. Czekanski, Mechanical characterization of additively manufactured parts by FE modeling of mesostructure, J. Manuf. Mater. Process. 1 (2017) 18, https://doi.org/10.3390/jmmp1020018.
[97] M. Somireddy, A. Czekanski, Anisotropic material behavior of 3D printed composite structures – material extrusion additive manufacturing, Mater. Des. 195 (2020), 108953, https://doi.org/10.1016/j.matdes.2020.108953.
[98] M. Somireddy, A. Czekanski, C.V. Singh, Development of constitutive material model of 3D printed structure via FDM, Mater. Today Commun. 15 (2018) 143–152, https://doi.org/10.1016/j.mtcomm.2018.03.004.
[99] M. Fernandez-Vicente, W. Calle, S. Ferrandiz, A. Conejero, Effect of infill parameters on tensile mechanical behavior in desktop 3D printing, 3D Print. Addit. Manuf. 3 (2016) 183–192, https://doi.org/10.1089/3dp.2015.0036.
[100] J. Podroužek, M. Marcon, K. Ninčević, R. Wan-Wendner, Bio-inspired 3D infill patterns for additive manufacturing and structural applications, Materials 12 (2019) 499, https://doi.org/10.3390/ma12030499.
[101] M.M. Hanon, R. Marczis, L. Zsidai, Anisotropy evaluation of different raster directions, spatial orientations, and fill percentage of 3D printed PETG tensile test specimens, Key Eng. Mater. 821 (2019) 167–173.
[102] K. Wang, X. Xie, J. Wang, A. Zhao, Y. Peng, Y. Rao, Effects of infill characteristics and strain rate on the deformation and failure properties of additively manufactured polyamide-based composite structures, Results Phys. 18 (2020), 103346, https://doi.org/10.1016/j.rinp.2020.103346.
[103] S. Terekhina, I. Skornyakov, T. Tarasova, S. Egorov, Effects of the infill density on the mechanical properties of nylon specimens made by filament fused fabrication, Technologies 7 (2019) 57, https://doi.org/10.3390/technologies7030057.
[104] M. Rismalia, S.C. Hidajat, I.G.R. Permana, B. Hadisujoto, M. Muslimin, F. Triawan, Infill pattern and density effects on the tensile properties of 3D printed PLA material, J. Phys.: Conf. Ser. 1402 (4) (2019), 044041, https://doi.org/10.1088/1742-6596/1402/4/044041.
[105] T.J. Suteja, A. Soesanti, Mechanical properties of 3D printed polylactic acid product for various infill design parameters: a review, J. Phys.: Conf. Ser. 1569 (4) (2020), 042010, https://doi.org/10.1088/1742-6596/1569/4/042010.

[106] L. Auffray, P.-A. Gouge, L. Hattali, Design of experiment analysis on tensile properties of PLA samples produced by fused filament fabrication, Int. J. Adv. Manuf. Technol. 118 (2022) 4123–4137, https://doi.org/10.1007/s00170-021-08216-7.
[107] K.L. Alvarez, R.F. Lagos, M. Aizpun, Investigating the influence of infill percentage on the mechanical properties of fused deposition modelled ABS parts, Ing. Invest. 36 (2016) 110–116, https://doi.org/10.15446/ing.investig.v36n3.56610.
[108] N. Elmrabet, P. Siegkas, Dimensional considerations on the mechanical properties of 3D printed polymer parts, Polym. Test. 90 (2020), 106656, https://doi.org/10.1016/j.polymertesting.2020.106656.
[109] J.C.P. Mena, E.R. Gallardo Vizuete, E.D.T. Peñaloza, Effect of the filling percentage on tensile strength in 3D desktop printing for different printing patterns, using a randomized design of experiments, Enfoque UTE 10 (2019) 13–27, https://doi.org/10.29019/enfoqueute.v10n4.503.
[110] S. Fafenrot, N. Grimmelsmann, M. Wortmann, A. Ehrmann, Three-dimensional (3D) printing of polymer-metal hybrid materials by fused deposition modeling, Materials 10 (2017) 1199, https://doi.org/10.3390/ma10101199.
[111] B. Gharehpapagh, M. Dolen, U. Yaman, Investigation of variable bead widths in FFF process, Procedia Manuf. 38 (2019) 52–59, https://doi.org/10.1016/j.promfg.2020.01.007.
[112] E.A. Papon, A. Haque, M.A.R. Sharif, Numerical study for the improvement of bead spreading architecture with modified nozzle geometries in additive manufacturing of polymers, Rapid Prototyp. J. 27 (2021) 518–529, https://doi.org/10.1108/RPJ-05-2019-0142.
[113] M.K. Agarwala, V.R. Jamalabad, N.A. Langrana, A. Safari, P.J. Whalen, S. C. Danforth, Structural quality of parts processed by fused deposition, Rapid Prototyp. J. 2 (1996) 4–19, https://doi.org/10.1108/13552549610732034.
[114] J.-F. Agassant, F. Pigeonneau, L. Sardo, M. Vincent, Flow analysis of the polymer spreading during extrusion additive manufacturing, Addit. Manuf. 29 (2019), 100794, https://doi.org/10.1016/j.addma.2019.100794.
[115] C. Luo, M. Mrinal, X. Wang, Y. Hong, Bonding widths of deposited polymer strands in additive manufacturing, Materials 14 (4) (2021) 871, https://doi.org/10.3390/ma14040871.
[116] P. Czyżewski, D. Marciniak, B. Nowinka, M. Borowiak, M. Bieliński, Influence of extruder's nozzle diameter on the improvement of functional properties of 3D-printed PLA products, Polymers 14 (2022) 356, https://doi.org/10.3390/polym14020356.
[117] T.J. Coogan, D.O. Kazmer, Modeling of interlayer contact and contact pressure during fused filament fabrication, J. Rheol. 63 (2019) 655–672, https://doi.org/10.1122/1.5093033.
[118] K. Savvakis, M. Petousis, A. Vairis, N. Vidakis, A.T. Bikmeyev, Experimental determination of the tensile strength of fused deposition modeling parts, in: Proceedings of the ASME 2014 International Mechanical Engineering Congress and Exposition, IMECE2014, Montreal, Quebec, Canada, November , https://doi.org/10.1115/IMECE2014-37553. IMECE2014-37553, V014T11A022.
[119] A. Lepoivre, A. Levy, N. Boyard, V. Gaudefroy, V. Sobotka, Coalescence in fused filament fabrication process: thermo-dependent characterization of high-performance polymer properties, Polym. Test. 98 (2021), 107096, https://doi.org/10.1016/j.polymertesting.2021.107096.
[120] D. Yang, H. Zhang, J. Wu, E.D. McCarthy, Fibre flow and void formation in 3D printing of short-fibre reinforced thermoplastic composites: an experimental benchmark exercise, Addit. Manuf. 37 (2021), 101686, https://doi.org/10.1016/j.addma.2020.101686.
[121] D.D. Phan, Z.R. Swain, M.E. Mackay, Rheological and heat transfer effects in fused filament fabrication, J. Rheol. 62 (2018) 1097–1107, https://doi.org/10.1122/1.5022982.
[122] C. Basgul, F.M. Thieringer, S.M. Kurtz, Heat transfer-based non-isothermal healing model for the interfacial bonding strength of fused filament fabricated polyetheretherketone, Addit. Manuf. 46 (2021), 102097, https://doi.org/10.1016/j.addma.2021.102097.
[123] J.T. Owens, A. Das, M.J. Bortner, Accelerating heat transfer modeling in material extrusion additive manufacturing: from desktop to big area, Addit. Manuf. 55 (2022), 102853, https://doi.org/10.1016/j.addma.2022.102853.
[124] H.J. O'Connor, D.P. Dowling, Evaluation of the influence of low pressure additive manufacturing processing conditions on printed polymer parts, Addit. Manuf. 21 (2018) 404–412, https://doi.org/10.1016/j.addma.2018.04.007.
[125] H.J. O'Connor, D.P. Dowling, Low-pressure additive manufacturing of continuous fiber-reinforced polymer composites, Polym. Compos. 40 (2019) 4329–4339, https://doi.org/10.1002/pc.25294.
[126] F. Lederle, F. Meyer, G.-P. Brunotte, C. Kaldun, E.G. Hübner, Improved mechanical properties of 3D-printed parts by fused deposition modeling processed under the exclusion of oxygen, Prog. Addit. Manuf. 1 (2016) 3–7, https://doi.org/10.1007/s40964-016-0010-y.
[127] S. Park, K.(K.) Fu, Polymer-based filament feedstock for additive manufacturing, Compos. Sci. Technol. 213 (2021), 108876, https://doi.org/10.1016/j.compscitech.2021.108876.
[128] M. Algarni, The influence of raster angle and moisture content on the mechanical properties of PLA parts produced by fused deposition modeling, Polymers 13 (2021) 237, https://doi.org/10.3390/polym13020237.
[129] A.D. Banjo, V. Agrawal, M.L. Auad, A.D.N. Celestine, Moisture-induced changes in the mechanical behavior of 3D printed polymers, Compos. Part C: Open Access 7 (2022), 100243, https://doi.org/10.1016/j.jcomc.2022.100243.
[130] S. Barone, P. Neri, S. Orsi, A. Paoli, A.V. Razionale, F. Tamburrino, Two coatings that enhance mechanical properties of fused filament-fabricated carbon-fiber reinforced composites, Addit. Manuf. 32 (2020), 101105, https://doi.org/10.1016/j.matdes.2017.03.065.
[131] V.M. Bruère, A. Lion, J. Holtmannspötter, M. Johlitz, Under-extrusion challenges for elastic filaments: the influence of moisture on additive manufacturing, Prog. Addit. Manuf. 7 (2022) 445–452, https://doi.org/10.1007/s40964-022-00300-y.
[132] S.N.A.M. Halidi, J. Abdullah, Moisture effects on the ABS used for fused deposition modeling rapid prototyping machine, in: 2012 IEEE Symposium on Humanities, Science and Engineering Research, 2012, pp. 839–843, https://doi.org/10.1109/SHUSER.2012.6268999.
[133] P. Kakanuru, K. Pochiraju, Moisture ingress and degradation of additively manufactured PLA, ABS and PLA/SiC composite parts, Addit. Manuf. 36 (2020), 101529, https://doi.org/10.1016/j.addma.2020.101529.
[134] E. Kim, Y.-J. Shin, S.-H. Ahn, The effects of moisture and temperature on the mechanical properties of additive manufacturing components: fused deposition modeling, Rapid Prototyp. J. 22 (2016) 887–894, https://doi.org/10.1108/RPJ-08-2015-0095.
[135] C. Ma, J. Faust, J.D. Roy-Mayhew, Drivers of mechanical performance variance in 3D-printed fused filament fabrication parts: an Onyx FR case study, Polym. Compos. 42 (2021) 4786–4794, https://doi.org/10.1002/pc.26187.
[136] N. Vidakis, M. Petousis, A. Maniadi, V. Papadakis, A. Manousaki, MEX 3D printed HDPE/TiO_2 nanocomposites physical and mechanical properties investigation, J. Compos. Sci. 6 (7) (2022) 209, https://doi.org/10.3390/jcs6070209.
[137] R. Anitha, S. Arunachalam, P. Radhakrishnan, Critical parameters influencing the quality of prototypes in fused deposition modelling, J. Mater. Process. Technol. 118 (2001) 385–388, https://doi.org/10.1016/S0924-0136(01)00980-3.
[138] A.A. Bakır, R. Atik, S. Özerinç, Mechanical properties of thermoplastic parts produced by fused deposition modeling: a review, Rapid Prototyp. J. 27 (2021) 537–561, https://doi.org/10.1108/RPJ-03-2020-0061.
[139] J.M. Chacón, M.A. Caminero, E. García-Plaza, P.J. Núnez, Additive manufacturing of PLA structures using fused deposition modelling: effect of process parameters on mechanical properties and their optimal selection, Mater. Des. 124 (2017) 143–157, https://doi.org/10.1016/j.matdes.2017.03.065.
[140] A. Dey, N. Yodo, A systematic survey of FDM process parameter optimization and their influence on part characteristics, J. Manuf. Mater. Process. 3 (2019) 64, https://doi.org/10.3390/jmmp3030064.
[141] J.R.C. Dizon, A.H. Espera Jr., Q. Chen, R.C. Advincula, Mechanical characterization of 3D-printed polymers, Addit. Manuf. 20 (2018) 44–67, https://doi.org/10.1016/j.addma.2017.12.002.
[142] K. Fayazbakhsh, M. Movahedi, J. Kalman, The impact of defects on tensile properties of 3D printed parts manufactured by fused filament fabrication, Mater, Today Commun 18 (2019) 140–148, https://doi.org/10.1016/j.mtcomm.2018.12.003.
[143] G.D. Goh, Y.L. Yap, H.K.J. Tan, S.L. Sing, G.L. Goh, W.Y. Yeong, Process-structure-properties in polymer additive manufacturing via material extrusion: a review, Crit. Rev. Solid State Mater. Sci. 45 (2020) 113–133, https://doi.org/10.1080/10408436.2018.1549977.
[144] M. Harris, J. Potgieter, R. Archer, K.M. Arif, Effect of material and process specific factors on the strength of printed parts in fused filament fabrication: a review of recent developments, Materials 12 (2019) 1664, https://doi.org/10.3390/ma12101664.
[145] H. Li, T. Wang, J. Sun, Z. Yu, The effect of process parameters in fused deposition modelling on bonding degree and mechanical properties, Rapid Prototyp. J. 24 (2018) 80–92, https://doi.org/10.1108/RPJ-06-2016-0090.
[146] O.A. Mohamed, S.H. Masood, J.L. Bhowmik, Optimization of fused deposition modeling process parameters: a review of current research and future prospects, Adv. Manuf. 3 (2015) 42–53, https://doi.org/10.1007/s40436-014-0097-7.
[147] T.N.A.T. Rahim, A.M. Abdullah, H.M. Akil, Recent developments in fused deposition modeling-based 3D printing of polymers and their composites, Polym. Rev. 59 (2019) 589–624, https://doi.org/10.1080/15583724.2019.1597883.
[148] V. Shanmugam, D.J.J. Rajendran, K. Babu, S. Rajendran, A. Veerasimman, U. Marimuthu, S. Singh, O. Dash, R.E. Neisiany, M.S. Hedenqvist, F. Berto, S. Ramakrishna, The mechanical testing and performance analysis of polymer-fibre composites prepared through the additive manufacturing, Polym. Test. 93 (2021), 106925, https://doi.org/10.1016/j.polymertesting.2020.106925.
[149] A.J. Sheoran, H. Kumar, Fused Deposition modeling process parameters optimization and effect on mechanical properties and part quality: review and reflection on present research, Mater. Today Proc. 21 (2020) 1659–1672, https://doi.org/10.1016/j.matpr.2019.11.296.
[150] A.K. Sood, R.K. Ohdar, S.S. Mahapatra, Parametric appraisal of mechanical property of fused deposition modelling processed parts, Mater. Des. 31 (2010) 287–295, https://doi.org/10.1016/j.matdes.2009.06.016.
[151] D. Syrlybayev, B. Zharylkassyn, A. Seisekulova, M. Akhmetov, A. Perveen, D. Talamona, Optimisation of strength properties of FDM printed parts—a critical review, Polymers 13 (2021) 1587, https://doi.org/10.3390/polym13101587.
[152] N.G. Tanikella, B. Wittbrodt, J.M. Pearce, Tensile strength of commercial polymer materials for fused filament fabrication 3D printing, Addit. Manuf. 15 (2017) 40–47, https://doi.org/10.1016/j.addma.2017.03.005.
[153] J.T. Cantrell, S. Rohde, D. Damiani, R. Gurnani, L. DiSandro, J. Anton, A. Young, A. Jerez, D. Steinbach, C. Kroese, P.G. Ifju, Experimental characterization of the mechanical properties of 3D-printed ABS and polycarbonate parts, Rapid Prototyp. J. 23 (2017) 811–824, https://doi.org/10.1108/RPJ-03-2016-0042.
[154] ASTM D638, ASTM D638-14. Standard Test Method for Tensile Properties of Plastics. Book of Standards Volume: 08.01, 2014, https://doi.org/10.1520/D0638-14. Developed by Subcommittee: D20.10.
[155] A. Özen, D. Auhl, C. Völlmecke, J. Kiendl, B.E. Abali, Optimization of manufacturing parameters and tensile specimen geometry for fused deposition

modeling (FDM) 3D-printed PETG, Materials 14 (2021) 2556, https://doi.org/10.3390/ma14102556.
[156] R.T.L. Ferreira, I.C. Amatte, T.A. Dutra, D. Bürger, Experimental characterization and micrography of 3D printed PLA and PLA reinforced with short carbon fibers, Compos. B Eng. 124 (2017) 88–100, https://doi.org/10.1016/j.compositesb.2017.05.013.
[157] A. Sola, A. Trinchi, 12 - fused deposition modeling of composite materials at a glance – supplementary tables. In: A. Sola, A. Trinchi, Fused Deposition Modeling of Composite Materials. Woodhead Publishing, Elsevier, Cambridge, MA, United States – Kidlington, UK, 329-444. DOI: 10.1016/B978-0-323-98823-0.00003-2.
[158] ISO 527-2, ISO 527-2:2012, Plastics — Determination of Tensile Properties — Part 2: Test Conditions for Moulding and Extrusion Plastics, Technical Committee ISO/TC 61/SC 2 Mechanical behavior, 2012.
[159] K. Raney, E. Lani, D.K. Kalla, Experimental characterization of the tensile strength of ABS parts manufactured by fused deposition modeling process, Mater. Today Proc. 4 (2017) 7956–7961, https://doi.org/10.1016/j.matpr.2017.07.132.
[160] A. Roschli, K.T. Gaul, A.M. Boulger, B.K. Post, P.C. Chesser, L.J. Love, B. Fletcher, M. Borish, Designing for big area additive manufacturing, Addit. Manuf. 25 (2019) 275–285, https://doi.org/10.1016/j.addma.2018.11.006.
[161] M. Milosevic, D. Stoof, K.L. Pickering, Characterizing the mechanical properties of fused deposition modelling natural fiber recycled polypropylene composites, J. Compos. Sci. 1 (2017) 7, https://doi.org/10.3390/jcs1010007.
[162] T.J. Prater, Q.A. Bean, R.D. Beshears, T.D. Rolin, N.J. Werkheiser, E.A. Ordonez, R.M. Ryan, F.E. Ledbetter III, Summary Report on Phase I Results from the 3D Printing in Zero-G Technology Demonstration Mission, vol. I, 2016. No. NASA/TP-2016-219101.
[163] T.J. Word, A. Guerrero, D.A. Roberson, Novel polymer materials systems to expand the capabilities of FDMTM-type additive manufacturing, MRS Commun 11 (2021) 129–145, https://doi.org/10.1557/s43579-021-00011-5.
[164] E. Gkartzou, E.P. Koumoulos, C.A. Charitidis, Production and 3D printing processing of bio-based thermoplastic filament, Manuf. Rev. 4 (2017) 1, https://doi.org/10.1051/mfreview/2016020.
[165] F. Ning, W. Cong, Y. Hu, H. Wang, Additive manufacturing of carbon fiber-reinforced plastic composites using fused deposition modeling: effects of process parameters on tensile properties, J. Compos. Mater. 51 (2017) 451–462, https://doi.org/10.1177/0021998316646169.
[166] F. Ning, W. Cong, Z. Hu, K. Huang, Additive manufacturing of thermoplastic matrix composites using fused deposition modeling: a comparison of two reinforcements, J. Compos. Mater. 51 (2017) 3733–3742, https://doi.org/10.1177/0021998317692659.
[167] A. Uşun, R. Gümrük, The mechanical performance of the 3D printed composites produced with continuous carbon fiber reinforced filaments obtained via melt impregnation, Addit. Manuf. 46 (2021), 102112, https://doi.org/10.1016/j.addma.2021.102112.
[168] A. García-Domínguez, J. Claver, A.M. Camacho, M.A. Sebastián, Considerations on the applicability of test methods for mechanical characterization of materials manufactured by FDM, Materials 13 (2020) 28, https://doi.org/10.3390/ma13010028.
[169] AENOR/UNE 116005, AENOR/UNE 116005. Fabricación por adición de capas en materiales plásticos. Fabricación aditiva. Preparación de probetas, AENOR, Madrid, Spain, 2012.
[170] V. Chandran, J. Kalman, K. Fayazbakhsh, H. Bougherara, A comparative study of the tensile properties of compression molded and 3D printed PLA specimens in dry and water saturated conditions, J. Mech. Sci. Technol. 35 (2021) 1977–1985, https://doi.org/10.1007/s12206-021-0415-5.
[171] D. Croccolo, M. De Agostinis, G. Olmi, Experimental characterization and analytical modelling of the mechanical behaviour of fused deposition processed parts made of ABS-M30, Comput. Mater. Sci. 79 (2013) 506–518, https://doi.org/10.1016/j.commatsci.2013.06.041.
[172] T. Letcher, M. Waytashek, Material property testing of 3D-printed specimen in PLA on an entry-level 3D printer, V02AT02A014. ASME, in: Proceedings of the ASME 2014 International Mechanical Engineering Congress and Exposition, 2AAdvanced Manufacturing. Montreal, Quebec, Canada, 2014, https://doi.org/10.1115/IMECE2014-39379. November 14–20.
[173] A. Miller, C. Brown, G. Warner, Guidance on the use of existing ASTM polymer testing standards for ABS parts fabricated using FFF, Smart Sustain. Manuf. Syst. 3 (2019) 122–138, https://doi.org/10.1520/SSMS20190051.
[174] M. Montero, S. Roundy, D. Odell, S.-H. Ahn, P.K. Wright, Material Characterization of Fused Deposition Modeling (FDM) ABS by Designed Experiments, Rapid Prototyping and Manufacturing Conference, Society of Manufacturing Engineers, 2001, p. 21.
[175] B. Rankouhi, S. Javadpour, F. Delfanian, T. Letcher, Failure analysis and mechanical characterization of 3D printed ABS with respect to layer thickness and orientation, J. Fail. Anal. Prev. 16 (2016) 467–481, https://doi.org/10.1007/s11668-016-0113-2.
[176] G.W. Melenka, B.K. Cheung, J.S. Schofield, M.R. Dawson, J.P. Carey, Evaluation and prediction of the tensile properties of continuous fiber-reinforced 3D printed structures, Compos. Struct. 153 (2016) 866–875, https://doi.org/10.1016/j.compstruct.2016.07.018.
[177] A.W. Gebisa, H.G. Lemu, Influence of 3D printing FDM process parameters on tensile property of ULTEM 9085, Procedia Manuf. 30 (2019) 331–338, https://doi.org/10.1016/j.promfg.2019.02.047.
[178] L. Pyl, K.-A. Kalteremidou, D. Van Hemelrijck, Exploration of specimen geometry and tab configuration for tensile testing exploiting the potential of 3D printing freeform shape continuous carbon fibre-reinforced nylon matrix composites, Polym. Test. 71 (2018) 318–328, https://doi.org/10.1016/j.polymertesting.2018.09.022.
[179] ASTM D3039, ASTM D3039/D3039M-17. Standard Test Method for Tensile Properties of Polymer Matrix Composite Materials. Book of Standards, 15.03, 2017, https://doi.org/10.1520/D3039_D3039M-17. Developed by Subcommittee: D30.04.
[180] ISO 527-4, ISO 527-4:2021, Plastics — Determination of Tensile Properties — Part 4: Test Conditions for Isotropic and Orthotropic Fibre-Reinforced Plastic Composites, Technical Committee ISO/TC 61/SC 13 Composites and reinforcement fibres, 2021.
[181] C. Wendt, S.R. Fernández-Vidal, Á. Gómez-Parra, M. Batista, M. Marcos, Processing and quality evaluation of additive manufacturing monolayer specimens, Adv. Mater. Sci. Eng. 2016 (2016), 5780693, https://doi.org/10.1155/2016/5780693.
[182] Z. Xu, R. Fostervold, S.M.J. Razavi, Scale effect on the mechanical behavior of PLA specimens fabricated via fused deposition modeling, Procedia Struct. Integr. 33 (2021) 564–570, https://doi.org/10.1016/j.prostr.2021.10.062.
[183] R.J. Zaldivar, D.B. Witkin, T. McLouth, D.N. Patel, K. Schmitt, J.P. Nokes, Influence of processing and orientation print effects on the mechanical and thermal behavior of 3D-Printed ULTEM® 9085, Material. Addit. Manuf. 13 (2017) 71–80, https://doi.org/10.1016/j.addma.2016.11.007.
[184] K. Chin Ang, K. Fai Leong, C. Kai Chua, M. Chandrasekaran, Investigation of the mechanical properties and porosity relationships in fused deposition modelling-fabricated porous structures, Rapid Prototyp. J. 12 (2006) 100–105, https://doi.org/10.1108/13552540610652447.
[185] C. Pagano, L. Rebaioli, F. Baldi, I. Fassi, Relationships between size and mechanical properties of scaffold-like structures, Mech. Adv. Mater. Struct. 28 (2021) 1812–1817, https://doi.org/10.1080/15376494.2019.1709675.
[186] J.M. Guerrero, J.A. Mayugo, J. Costa, A. Turon, Size effects in hybrid unidirectional polymer composites under longitudinal tension: a micromechanical investigation, Compos. Part A Appl. Sci. Manuf. 140 (2021), 106186, https://doi.org/10.1016/j.compositesa.2020.106186.
[187] C. Wendt, M. Batista, E. Moreno, A.P. Valerga, S.R. Fernández-Vidal, O. Droste, M. Marcos, Preliminary design and analysis of tensile test samples developed by additive manufacturing, Procedia Eng. 132 (2015) 132–139, https://doi.org/10.1016/j.proeng.2015.12.489.
[188] T.T. Zhu, A.J. Bushby, D.J. Dunstan, Materials mechanical size effects: a review, Mater. Technol. 23 (2008) 193–209, https://doi.org/10.1179/175355508X376843.
[189] Z.P. Bažant, Size effect on structural strength: a review, Arch. Appl. Mech. 69 (1999) 703–725, https://doi.org/10.1007/s004190050252.
[190] S. Nikolov, C.S. Han, D. Raabe, On the origin of size effects in small-strain elasticity of solid polymers, Int. J. Solid Struct. 44 (2007) 1582–1592, https://doi.org/10.1016/j.ijsolstr.2006.06.039.
[191] T. Amornsakchai, D.L.M. Cansfield, S.A. Jawad, G. Pollard, I.M. Ward, The relation between filament diameter and fracture strength for ultra-high-modulus polyethylene fibres, J. Mater. Sci. 28 (1993) 1689–1698, https://doi.org/10.1007/BF00363369.
[192] J.N. Baucom, A. Rohatgi, W.R. Pogue, J.P. Thomas, Characterization of a multifunctional liquid crystalline polymer nanocomposite, in: Presented at the 2005 SEM Annual Conference & Exposition on Experimental and Applied Mechanics, 2005. Portland, OR.
[193] Ż. Górecka, J. Idaszek, D. Kołbuk, E. Choińska, A. Chlanda, W. Święszkowski, The effect of diameter of fibre on formation of hydrogen bonds and mechanical properties of 3D-printed PCL, Mater. Sci. Eng. C 114 (2020), 111072, https://doi.org/10.1016/j.msec.2020.111072.
[194] P.K. Penumakala, J. Santo, A. Thomas, A critical review on the fused deposition modeling of thermoplastic polymer composites, Compos. B Eng. 201 (2020), 108336, https://doi.org/10.1016/j.compositesb.2020.108336.
[195] P. Zhang, Z. Wang, J. Li, X. Li, L. Cheng, From materials to devices using fused deposition modeling: a state-of-art review, Nanotechnol. Rev. 9 (2020) 1594–1609, https://doi.org/10.1515/ntrev-2020-0101.
[196] C.M. Vicente, T.S. Martins, M. Leite, A. Ribeiro, L. Reis, Influence of fused deposition modeling parameters on the mechanical properties of ABS parts, Polym. Adv. Technol. 31 (2020) 501–507, https://doi.org/10.1002/pat.4787.
[197] D. Drummer, S. Cifuentes-Cuéllar, D. Rietzel, Suitability of PLA/TCP for fused deposition modeling, Rapid Prototyp. J. 18 (2012) 500–507, https://doi.org/10.1108/13552541211272045.
[198] Z. Decker, M. Makulinski, S. Vispute, M. Sundaram, Effects of size reduction on the failure mechanism of 3D printed PLA+ parts, in: Proceedings of the ASME 2021 16th International Manufacturing Science and Engineering Conference, MSEC2021, June 21-25, 2021, Virtual, On-Line, American Society of Mechanical Engineers, 2021 eid: V001T01A028.
[199] A.R. Aziz, J. Zhou, D. Thorne, W.J. Cantwell, Geometrical scaling effects in the mechanical properties of 3D-printed body-centered cubic (BCC) lattice structures, Polymers 13 (2021) 3967, https://doi.org/10.3390/polym13223967.
[200] D. Bell, T. Siegmund, 3D-printed polymers exhibit a strength size effect, Addit. Manuf. 21 (2018) 658–665, https://doi.org/10.1016/j.addma.2018.04.013.
[201] C. Vălean, L. Marşavina, M. Mărghitaş, E. Linul, J. Razavi, F. Berto, Effect of manufacturing parameters on tensile properties of FDM printed specimens, Procedia Struct. Integr. 26 (2020) 313–320, https://doi.org/10.1016/j.prostr.2020.06.040.
[202] ISO 527-1, ISO 527-1:2019, Plastics — Determination of Tensile Properties — Part 1: General Principles, Technical Committee: ISO/TC 61/SC 2 Mechanical behavior, 2019.

[203] S. Guessasma, S. Belhabib, H. Nouri, O.B. Hassana, Anisotropic damage inferred to 3D printed polymers using fused deposition modelling and subject to severe compression, Eur. Polym. J. 85 (2016) 324–340, https://doi.org/10.1016/j.eurpolymj.2016.10.030.

[204] C. Kung, H.-C. Kuan, C.-F. Kuan, Evaluation of tensile strength of 3D printed objects with FDM process on RepRap platform, in: 1st IEEE International Conference on Knowledge Innovation and Invention 2018, 2018, pp. 369–372, https://doi.org/10.1109/ICKII.2018.8569166. Jeju (Korea (South)), July 23-27.

[205] ISO 37, ISO 37:2017 Rubber, Vulcanized or Thermoplastic — Determination of Tensile Stress-Strain Properties, Technical Committee: ISO/TC 45/SC 2 Testing and analysis, 2017.

[206] ISO 3167, ISO 3167:2014, Plastics — Multipurpose Test Specimens, Technical Committee: ISO/TC 61/SC 2 Mechanical behavior, 2014.

[207] A. Bellini, S. Güçeri, Mechanical characterization of parts fabricated using fused deposition modeling, Rapid Prototyp. J. 9 (2003) 252–264, https://doi.org/10.1108/13552540310489631.

[208] D. Stoof, K. Pickering, 3D printing of natural fibre reinforced recycled polypropylene, in: Processing and Fabrication of Advanced Materials-XXV, The University of Auckland, Auckland (New Zealand), 2017, pp. 668–691.

[209] S. Berretta, R. Davies, Y.T. Shyng, Y. Wang, O. Ghita, Fused deposition modelling of high temperature polymers: exploring CNT PEEK composites, Polym. Test. 63 (2017) 251–262, https://doi.org/10.1016/j.polymertesting.2017.08.024.

[210] G.C. Jacob, J.M. Starbuck, J.F. Fellers, S. Simunovic, R.G. Boeman, Strain rate effects on the mechanical properties of polymer composite materials, J. Appl. Polym. Sci. 94 (2004) 296–301, https://doi.org/10.1002/app.20901.

[211] C.R. Siviour, J.L. Jordan, High strain rate mechanics of polymers: a review, J. Dyn. Behav. Mater. 2 (2016) 15–32, https://doi.org/10.1007/s40870-016-0052-8.

[212] N. Vidakis, M. Petousis, E. Velidakis, M. Liebscher, V. Mechtcherine, L. Tzounis, On the strain rate sensitivity of fused filament fabrication (FFF) processed PLA, ABS, PETG, PA6, and PP thermoplastic polymers, Polymers 12 (2020) 2924, https://doi.org/10.3390/polym12122924.

[213] J.F. Rodríguez, J.P. Thomas, J.E. Renaud, Mechanical behavior of acrylonitrile butadiene styrene (ABS) fused deposition materials, Experimental investigation, Rapid Prototyp. J. 7 (2001) 148–158, https://doi.org/10.1108/13552540110395547.

[214] V. Cojocaru, D. Frunzaverde, C.O. Miclosina, G. Marginean, The influence of the process parameters on the mechanical properties of PLA specimens produced by fused filament fabrication—a review, Polymers 14 (5) (2022) 886, https://doi.org/10.3390/polym14050886.

[215] T. Mengesha Medibew, A comprehensive review on the optimization of the fused deposition modeling process parameter for better tensile strength of PLA-printed parts, Adv. Mater. Sci. Eng. 2022 (2022), 5490831, https://doi.org/10.1155/2022/5490831.

[216] Z. Liu, Y. Wang, B. Wu, C. Cui, Y. Guo, C. Yan, A critical review of fused deposition modeling 3D printing technology in manufacturing polylactic acid parts, Int. J. Adv. Manuf. Technol. 102 (9) (2019) 2877–2889, https://doi.org/10.1007/s00170-019-03332-x.

[217] PLA3D850 datasheet, Available on-line: https://www.natureworksllc.com/~/media/Files/NatureWorks/Technical-Documents/Technical-Data-Sheets/TechnicalDataSheet_3D850_monofilament_pdf.pdf. (Accessed 19 August 2022).